UNIVERSITY OF OKLAHOMA

GRADUATE COLLEGE

CHARACTERIZATION OF POLYETHOXYLATED ALKYL PHENOLS WITH A HIGH DEGREE OF ETHOXLYATION AT THE SOLID-LIQUID INTERFACE

A DISSERTATION

SUBMITTED TO THE GRADUATE FACULTY

in partial fulfillment of the requirements for the

Degree of

DOCTOR OF PHILOSOPHY

By

DANIELLE KIMBERLY BAKER
Norman, Oklahoma
2016

CHARACTERIZATION OF POLYETHOXYLATED ALKYL PHENOLS WITH A HIGH DEGREE OF ETHOXYLATION AT THE SOLID-LIQUID INTERFACE

A DISSERTATION APPROVED FOR THE
SCHOOL OF CHEMICAL, BIOLOGICAL AND MATERIALS ENGINEERING

BY

_____
Dr. Jeffrey H. Harwell, Chair

_____
Dr. Lance L. Lobban

_____
Dr. Edgar A. O'Rear III

_____
Dr. David. A. Sabatini

_____
Dr. Bor-Jier (Ben) Shiau

Dedicated to David, Daniel, Karen, Kent, Elizabeth, Kimberly, Aristotle, Alexander, and Andromeda.

Acknowledgements

The author of this paper would like to thank the following:

Thank you to Dr. Harwell. This dissertation would not have been possible without your confidence and advice.

Thank you to Dr. Shiau, Dr. Sabatini, Dr. Lobban, and Dr. O'Rear. Your support and encouragement throughout this dissertation has been greatly appreciated.

Thank you to Michael Bendrick. Your wealth of knowledge and reliable work helped make this paper possible.

Thank you to the Asahi Glass Foundation Chair in Chemical Engineering at the University of Oklahoma for funding this work.

Table of Contents

List of Tables

List of Figures

Abstract

Fully characterizing the behavior of a surfactant, from the mechanism of adsorption to the formation of micelles, is vital when taking the surfactant out of the lab and into the real world. The critical micelle concentration, cloud point, and mechanism of adsorption are only a few aspects of a nonionic surfactant that must be understood. For nonionic surfactant solutions, the solution properties can change depending on the system temperature, salt concentration, salt type, etc. This dissertation focuses on the adsorption of high polyethoxylated alkyl phenols, more than 25 ethylene oxide units, on the hydrophilic silica surface and how environmental conditions affect the surfactant adsorption at the solid-liquid interface. The effects of ions of different salts on the adsorption densities and the shape of developed adsorption isotherms are related to the Hofmeister series. Depending on the ions present in solution, the maximum adsorption density is shown to increase or decrease in accordance with the Hofmeister series's classification of ion as salting in or salting out. The salting out effect of sodium chloride causing an increase in adsorption density as well as a decrease in nonionic surfactant cloud points is examined as a fraction fluid, containing a high polyethoxylated alky phenol, travels through a packed ground shale or sand column. The effect of sodium chloride on a select few ionic surfactants traveling through the same packed ground shale or sand column is also analyzed. For the high polyethoxylated alky phenols, the formation of a coacervate hindered the surfactant migrating to the end of the column. For the ionic surfactants, the migration to the end of the packed column varied depending on the surfactant's salt and temperature tolerance. Lastly, evidence is given with UV, quartz crystal microbalance, and

ellipsometry analysis for a different mechanisms of adsorption for polyethoxylated alky phenols with a high degree of ethoxylation versus a low degree of ethoxylation.

Keywords – Ethoxylated Nonionic Surfactants, High Salinity Brine, Hofmeister Series, Cloud Point, Coacervate, Fracturing Fluid, Adsorbed Layer Thickness

Chapter 1: Introduction

Current working theories hypothesize that coacervates, the colloid particle rich phase in an aqueous liquid phase separation, not only pre-date living organisms but played a vital role in the origins of life on earth.[1,2] As the significance and applications of coacervates continues to grow, there are still many questions about their behavior. This paper focuses on nonionic surfactant adsorption and how the formation of a coacervate relates to adsorption at the solid-liquid interface.

Coacervate properties become relevant when discussing the potential of hydraulic fracturing fluid to contaminate ground water. Hydraulic fracturing fluid is mostly composed of water and sand; however, one-half to two percent of the fluid is composed of chemicals necessary to enhance the effectiveness of the fracturing process.[3] These chemicals can be acids, gelling agents, surfactants, preservatives, scale inhibitors, etc.[4] The fate of these chemicals after injection is a serious public concern.[5] From fracturing fluid formulation to risk assessment of groundwater contamination, the high temperatures and electrolyte concentrations of oil and gas reservoir brine must be considered fully. Temperature and electrolyte concentration can drastically affect the behavior of a surfactant injected into a reservoir. A thorough understanding of surfactant behavior under reservoir conditions is vital to knowing the effectiveness of fracturing fluids and their fate post-injection.

In oil reservoirs, the behavior of surfactants at the oil-water interface and the solid-liquid interface is crucial to the success of a surfactant system post injection. In 1982, Beunen and Ruckenstein published a paper[6] covering the effect of salting out for nonionic surfactants at the oil-water interface. This paper explains in detail how the

presence of salts and the hydrophilic-lipophilic balance (HLB) of nonionic surfactants with a low degree of ethoxylation, less than 10, decreases the interfacial tension at the liquid-liquid interface. From this work, it is clear that the presence of salts cannot be neglected when characterizing nonionic surfactant behavior at an interface. Placing a similar emphasis on salt concentration, this paper also aims to summarize the effect of different electrolytes on nonionic surfactant adsorption at the solid-liquid interface.

Adsorption Behavior

As surfactant adsorbs at the oil-water interface, interfacial tension is decreased. This phenomena has been well documented[6,7] for both ionic and nonionic surfactants. This type of adsorption is desirable in oil extraction applications and increases with temperature and salinity. At the solid-liquid interface, surfactant adsorption is undesirable in oil extraction and ground water remediation applications and contributes to the loss of effectiveness of a surfactant system. Nonionic polyethoxylated surfactants containing a low degree of ethoxylation, 25 or fewer ethylene oxide (EO) groups, adsorbing at the silica-water interface, have been thoroughly examined[8-24]. While the amount of literature concerning adsorption of higher ethoxylated surfactants is not as significant, several papers contain information about adsorption isotherms[8,9,12,16], calorimetric effects[10], and adsorbed layer thickness[18] for a nonionic surfactant with an ethoxylate number greater than 25 on silica.

Distinction between Low and High Degree of Ethoxylation

Appreciation for the distinction between adsorption of low and high ethoxylated nonionic surfactants is gained through observing the difference in shape of their adsorption isotherms on silica. The different isotherm shapes can be seen in Figure 1.

Adsorption isotherms for nonionic surfactants with a low degree of ethoxylation on a hydrophilic surface are best described as S-shaped or Modified-Langmuir isotherms. Examples of this type of isotherm are nonylphenol polyethoxylated (10), NP-10, in Figure 1. Initially, adsorption is characterized by monomeric adsorption obeying Henry's Law (constant slope = 1 on a log-log plot). This monomeric adsorption is due to the hydrogen bonding between the ethylene oxide units of the nonionic surfactant and the hydroxyl groups on the silica surface.[8,16] At higher surfactant concentrations, there is a steep increase in adsorption density (slope > 1 on a log-log plot) due to the onset of lateral hydrophobic association among surfactants, resulting in surface aggregates. The concentration at which the lateral hydrophobic association begins is frequently referred to as the critical surface aggregation concentration, CSAC. As surface coverage increases, the rate of adsorption decreases because only less energetically favorable surface sites are available for adsorption. Lastly, there is a plateau in the adsorption isotherm indicating that maximum surface coverage or the critical micelle concentration, CMC, has been reached. To good approximation the monomer-micelle equilibrium can be treated as a phase equilibrium, with the micelles serving as the liquid phase and the monomers as the gas phase. This approach to monomer-micelle equilibrium is called the pseudophase separation model and is adequate to explain many commonly observed surfactant phenomena, including the adsorption plateau at both the solid-liquid and the liquid-gas interfaces. The state of the adsorbed layer in the plateau region has been described either as clusters of surface aggregates or as bilayer-like. Figure 2 shows a simple schematic of surfactant interfacial behavior at the different stages of adsorption for polyethoxylated surfactants with a low degree of ethoxylation:

individual monomers adsorb in Region I; surface aggregates fill the most energetically favorable surface sites in Region II; less energetically favorable sites are infilled in Region III; and the onset of micelle formation in the bulk occurs in Region IV.

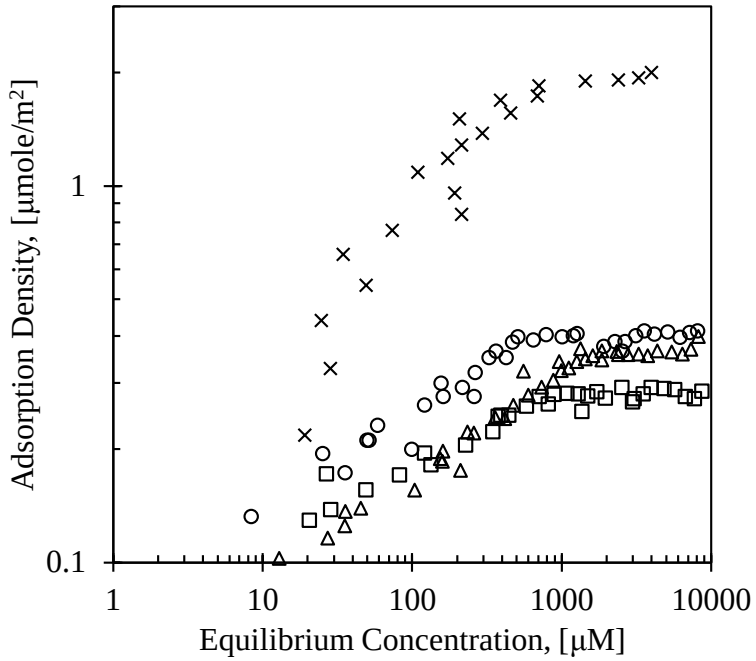

Figure 1: Adsorption isotherms for OP-40 (△), NP-40 (○), NP-55 (□), NP-10 (x) developed at 30°C in deionized water with fumed silica.

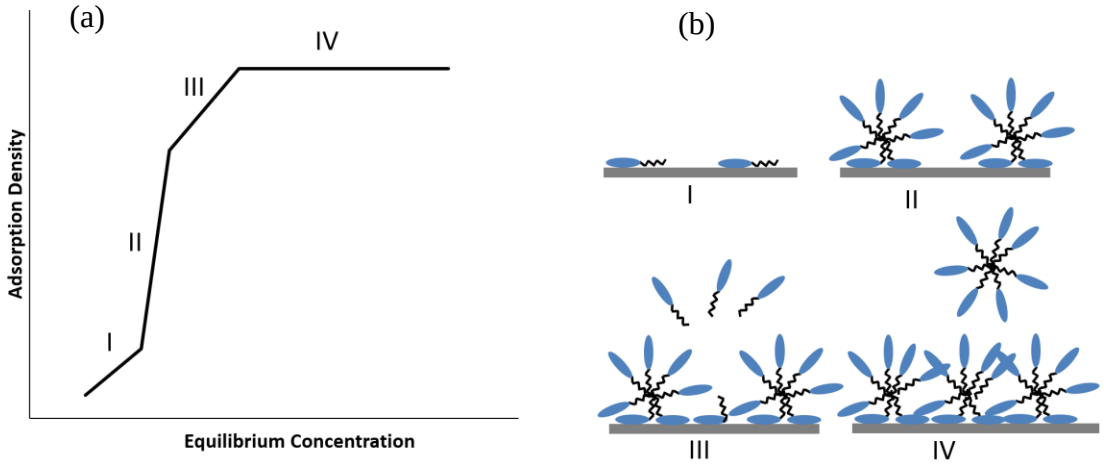

Figure 2: (a) Adsorption isotherm of nonionic surfactant with less than 25 EO units. Different stages of adsorption are marked by I-III. (b) Schematic of nonionic surfactants adsorbing at the solid-liquid interface during stages I-III of adsorption.

For nonionic surfactants with a high degree of ethoxylation, the size of the hydrophilic ethylene oxide head group sterically hinders lateral hydrophobic alkyl interaction among the adsorbed nonionic surfactants. This steric hindrance prevents the previously described adsorption mechanism of formation of surface aggregates in region two, thus leaving the surface at the stage of monomeric coverage, after a two-step adsorption process, when the bulk concentration reaches the CMC of the surfactant.[8,9] An example of this type of adsorption isotherm is seen in Figure 1 for octylphenol polyethoxylate (40), OP-40, and nonlyphenol ethoxylates NP-40 and NP-55. A schematic of the nonionic surfactant adsorption stages for highly ethoxylated nonionic surfactants is shown in Figure 3

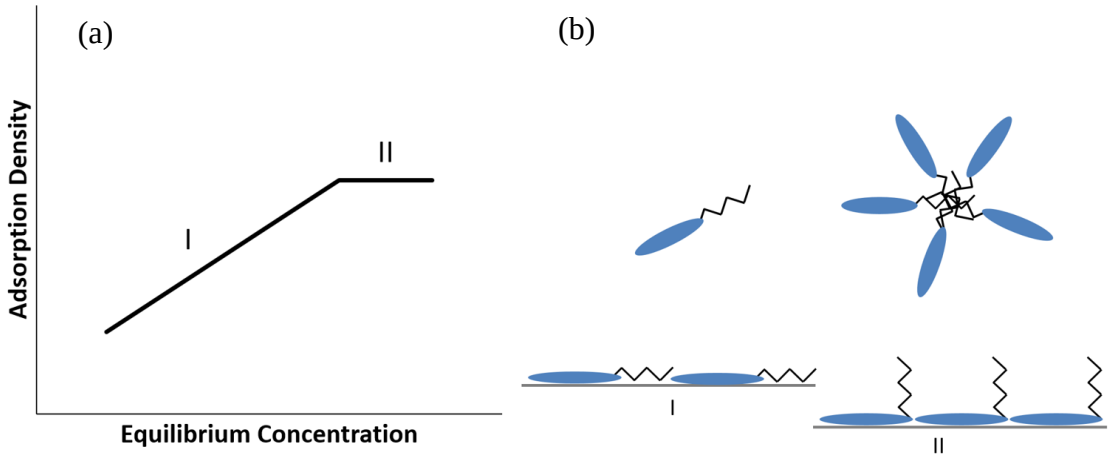

Figure 3: (a) Adsorption isotherm of nonionic surfactant with greater than 25 EO units. Different stages of adsorption are marked by I-II. (b) Schematic of nonionic surfactants adsorbing at the solid-liquid interface during stages I-II of adsorption.

Further distinction between adsorption of high and low ethoxylated surfactants is seen through calorimetric evidence published by Lindheimer, et al.[10] At surface coverage of less than 0.1 monolayers, adsorption of the polar ethoxylate chains onto the hydrophilic silica surface is exothermic. Between 0.1 to 0.3 monolayers surface

coverage, the second interaction of lateral alkyl-alkyl interaction is observed for surfactants with a low degree of ethoxylation. This endothermic interaction, a phenomenon characteristic of hydrophobic bonding, is similar to the interaction between the hydrophobic tails of surfactants in micelle formation and strongly indicates the onset of formation of micelle-like surface aggregates among the adsorbed surfactant. As surface coverage continues to increase beyond the 0.1 to 0.3 range, the overall differential enthalpy continues to change from exothermic to endothermic, eventually reaching an endothermic plateau. This endothermic plateau signifies the formation of surface aggregates and was observed for surfactant with a degree of ethoxylation between 9 and 16; however, for surfactants with a degree of ethoxylation of 30 and 40, no endothermic plateau was observed.[10] This observation is in accord with the previous comment on the steric hindrance by the long ethoxylate chains preventing alkyl-alkyl interaction in the adsorbed layer and thus inhibiting surface aggregate formation. Apparently, for nonionic surfactants with a high degree of ethoxylation, the strong exothermic interaction of the ethoxy chain with the silica surface so dominates the adsorption process that little if any hydrophobic bonding between surfactant alkyl chains can occur.

Influence of Hydrophilic-Lipophilic Balance

Details about the adsorption isotherm shape for a nonionic surfactant on hydrophilic silica can be inferred from the surfactant's hydrophilic-lipophilic balance (HLB). For the nonionic surfactants discussed in this paper, the HLB can be approximated as E/5, where E is the weight percent of ethylene oxide.[7] At low equilibrium concentrations, the adsorption density increases with longer ethylene oxide

chains, which is equivalent to a higher HLB number. At these low concentrations, adsorption takes place through hydrogen bonding between the ethoxylate units of the surfactant and the silanol groups of the hydrophilic silica surface. The longer ethylene oxide chains allow for strong adsorption on the surface, and thus greater low concentration adsorption density. Nonionic surfactants with an ethoxylate chain of 25 or less (surfactant with a lower HLB number, which implies a longer alkyl chain length and shorter ethylene oxide chain) produce a steeper first and second stage of adsorption. This indicates increasing strength of the lateral alkyl-alkyl association for more hydrophobic surfactants. This behavior is seen in Figure 1 for NP-10, NP-15, and NP-20. The isotherm plateau onset shifts to greater equilibrium concentrations for more hydrophilic surfactants, longer ethylene oxide chains, or a shorter alkyl chain. For surfactants with a degree of ethoxylation of 25 or less, the shorter ethoxy chains result in a lower critical surface aggregation concentration, i.e., lateral surfactant alkyl-alkyl interactions are occurring at lower concentrations, and thus the onset of the isotherm plateau occurs at lower concentrations. Longer ethylene oxide chains make the surfactant more hydrophilic and result in a higher critical micelle concentration. When the CMC is higher, the onset of the isotherm plateau is higher because adsorption will occur until monomeric activity is limited in solution by micelle formation.[10,16] The adsorption density decreases with an increasing degree of ethoxylation and becomes independent of the alkyl chain length. This indicates that the surface packing of these high HLB nonionic surfactants is governed by the degree of ethoxylation. As the degree of ethoxylation increases, the packing area per molecule increases and results in a lower molar adsorption density at the plateau.

Critical Micelle Concentration and Cloud Point

From the above observations, it is clear that knowledge of a surfactant's molecular structure gives insight into the hydrophilic and hydrophobic forces that play a role in the mechanism of adsorption and maximum adsorption density, as these forces also play a role in trends observed in the CMC and the upper consolute temperature for nonionic surfactants. The CMC is the surfactant solution concentration above which the surfactant monomers in the bulk solution aggregate and form micelles. Surfactants with a high HLB number, longer ethoxylate chain or shorter alkyl chain, have a higher CMC, while surfactants with a lower HLB number, shorter ethoxylate chain or longer alky chain, have a lower CMC.

The upper consolute temperature, or cloud point, is a solubility property associated with the coacervation of the nonionic surfactant. As temperature increases, the polyethoxylate chain of a nonionic surfactant is increasingly dehydrated until, at the upper consolute temperature, the surfactant micelles further aggregate and separate out of solution forming an aqueous surfactant-rich phase called a coacervate phase.[32] While the cloud point does increase with increasing EO number, Schott et al.[36] showed that there is an upper bound on the upper consulate temperature of polyethoxylated alcohols as the EO number increases. Nonionic surfactants with approximately 25 EO units, or more, converge with increasing EO number to an upper consulate temperature between 114 and 118 °C. To further emphasize the significance of the hydrophilic and hydrophobic character in these surfactant properties, Fineman et al.[25] noted that in the case of coacervation, the increase in a surfactant's hydrophobic character by the addition of one methylene group could be balanced out by the addition of one ethylene

oxide unit. Hsiao et.al.[26] noted, however, that the addition of one methylene group would decrease the CMC and require the addition of 12 ethylene oxide units to counterbalance the decrease in free energy when bringing a methylene group from the bulk solution to the interior of a micelle. This difference emphasizes that while the formation of micelles is driven by the removal of the alkyl chain from water, in the formation of the coacervate the alkyl chain is already removed from the water, and the issue is the coalescence of the micelles into a new, colloid-rich aqueous phase.

Influence of Salts

When a salt is present in solution with a polyethoxylated alkyl phenol surfactant, the ions affect the solubility of the surfactant and the formation of a coacervate;[26,27-39] it is generally believed that this effect occurs by the structuring or de-structuring of the water molecules in solution. The ions and their effect are classified as either kosmotropic or chaotropic. Kosmotropic, or structure-making ions are small, well hydrated ions with a high charge density that organize water molecules into small clusters through hydrogen bonding. The equilibrium between free water molecules and small, organized clusters of water molecules can be represented by the following equation.[39]

$$n H_2O \leftrightarrow (H_2O)_n \quad \textbf{(1)}$$

When kosmotropic ions are present in solution with polyethoxylated nonionic surfactants, the two compete with each other for water molecules to hydrogen bond with. This competition causes an aqueous solution with kosmotropic ions to be less solubilizing to a nonionic surfactant, compared to pure water; a phenomena known as salting out. Chaotropic, or structure-breaking, ions are large, less hydrated ions with a weak charge density that disrupts the organization of water molecules. The

disorganized water molecules are more available for hydrogen bonding with the polyethoxylated nonionic surfactants creating a salting-in effect by the chaotropic ions. The extent to which an ion displays a kosmotropic or chaotropic effect follows the Hofmeister series[31]; for polyethoxylated surfactants, however, an exception is made for Li^+ and all polyvalent cations, which are capable of forming complexes with the ethylene oxide chain, and which thereby increase the solubility of the polyethoxylated phenol.[30]

Because the presence of salts can affect the hydration of a nonionic surfactant, the surfactant's solubility and adsorption properties will also be affected. The extent to which the surfactant is hydrated can be related to the surfactant's upper consolute temperature and the critical micelle concentration.[39] For a polyethoxylated alkyl phenol, when the surfactant is more hydrated due to the presence of a chaotropic ion, the surfactant monomer solubility, the CMC, and the cloud point increase. When the surfactant is less hydrated due to the presence of a kosmotropic ion, then the surfactant solubility, the CMC, and the cloud point decrease. For example, sodium nitrate is composed of two salting-out ions and the effect of increasing salt concentration is apparent as the CMC decreases from 0.015 % (w/w) in deionized water to 0.013 % then 0.006 % (w/w) when the sodium nitrate concentration is increased to 1M and then to 3M, respectively.[30] However, cadmium nitrate has a salting-in effect due to the polyvalent cadmium ion having a salting-in effect on the nonionic surfactant. At low cadmium nitrate concentration, the salting-out effect of the nitrate ion is dominate as the CMC is almost unchanged, but as the salt concentration increases to 2M, the salting-in effect of the cadmium ion becomes dominate and the CMC increases to 0.022 % (w/w).

Several studies[33-36, 39] have investigated the effects different inorganic electrolytes have on the cloud points of nonionic surfactants and related the findings to the same properties that are responsible for changes in the critical micelle concentration of polyethoxylated surfactants. One paper[34] reported different salts having different effects and increasing salt concentration having an increasing effect on the cloud point of two linear secondary ethoxylated alcohol with 7 ethylene oxide units, one with 13.5 carbons and the other with 13 carbons. Both sodium sulfate and sodium phosphate had a salting out effect, decreasing the cloud point approximately 30°C at 0.400 M salt because the sodium, sulfate, and phosphate ions are all classified as salting-out in the Hofmeister series. Sodium iodide, on the other hand, is composed of sodium which is a weakly salting-out ion and iodide which is a strongly salting-in ion, resulting in an increase in cloud point by 5°C at 0.600 M salt. The different ion effects on the cloud point have been shown to be algebraically additive and can be normalized on a molar basis.[33]

Model for Adsorption at the Solid/Liquid Interface

Low Degree of Ethoxylation

For the case of adsorption of polyethoxylated surfactants with a degree of ethoxylation of 25 or less, a mass-action model was proposed by Gu et. al.[13] This model operates under the assumption that surfactant adsorption on a surface site (S) and the aggregation of *n* monomers forming surface aggregates (agg) takes place in one step. At equilibrium,

$$S + n\,\text{monomer} \rightleftarrows \text{surface aggregate} \qquad \textbf{(2)}$$

and

$$K = \frac{a_{agg}}{a_S a^n} \quad \textbf{(3)}$$

where K is the equilibrium constant; a is the activity of nonionic surfactant monomers in solution and for dilute solutions $a = c$, i.e. when the surfactant concentration is less than the CMC the surfactant activity is equal to the concentration of the surfactant; a_{agg} and a_S are the activities of the surface aggregates and surface sites and can be approximated as

$$a_{agg} = \frac{\Gamma}{n} \quad \textbf{(4)}$$

and

$$a_S = \frac{\Gamma_\infty - \Gamma}{n} \quad \textbf{(5)}$$

where Γ is the surfactant adsorption density at c and Γ_∞ is the maximum surface excess concentration achievable only at infinite surfactant concentration. Substituting equations (4) and (5) into equation (3) yields

$$\boldsymbol{K = \frac{\Gamma}{(\Gamma_\infty - \Gamma)\, c^n}} \quad \textbf{(6)}$$

Rearranging equation (6) results in the relation

$$\boldsymbol{\Gamma = \frac{\Gamma_\infty K c^n}{1 + K c^n}} \quad \textbf{(7)}$$

Equation (7) can be linearized and the parameters n and K can be calculated from the linear slope and y-intercept, respectively.

$$\log \frac{\Gamma}{\Gamma_\infty - \Gamma} = \log K + n \log c \quad \textbf{(8)}$$

Gu et. al.[13] demonstrated that the model's predictions worked very well on experimental adsorption data developed with Triton TX-100 (a branched octylphenol with an average of 9.5 EO units) on narrow and wide pore silica.

High Degree of Ethoxylation

A mass action model following a similar derivation is currently being investigated for nonionic surfactants with a degree of ethoxylation of 25 or greater.[41,42] In this model, instead of one surface site interacting with multiple surfactants, it is proposed that one surfactant interacts with multiple surface sites. At equilibrium,

$$\boldsymbol{p}\ \mathrm{S} + \mathrm{monomer} \rightleftarrows p\,\mathrm{S}^* \qquad \textbf{(9)}$$

and

$$K = \frac{a_{S^*}}{a_S a^{\frac{1}{p}}} \qquad \textbf{(10)}$$

where K is the equilibrium constant, p is the average number of surface sites, S, interacting with a monomer, and S* is the occupied surface sites. The model posits that the long EO chain of the highly ethoxylated surfactant covers multiple adsorption sites, preventing the nucleation of admicelles on those sites. This equilibrium assumption results in the adsorption isotherm Equation 11, where the variables are the same as mentioned above.

$$\boldsymbol{\Gamma} = \frac{\Gamma_\infty K c^{\frac{1}{p}}}{1 + K c^{\frac{1}{p}}} \qquad \textbf{(11)}$$

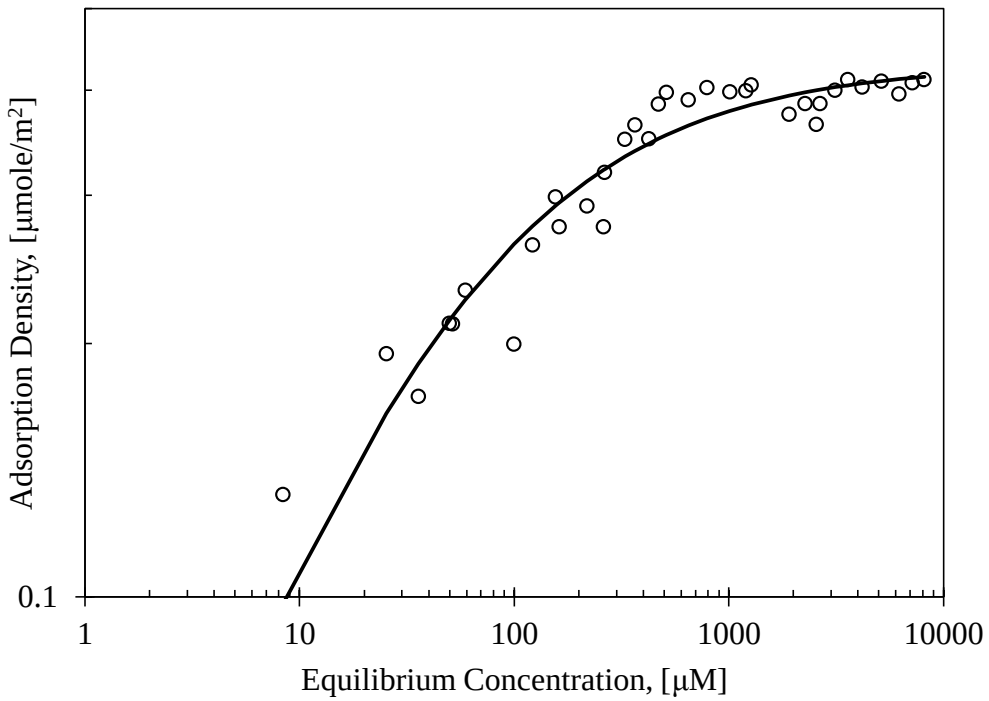

Figure 4: Comparison between the adsorption isotherm for NP-40 on fumed silica in deionized water at 30°C and the mass action model for nonionic surfactants with a high degree of ethoxylation (—)

Normalization of Adsorption Isotherms

Because trends were observed in mechanism of adsorption, maximum adsorption density, CMC, and cloud point, based on the surfactant's HLB, two papers[11,40] demonstrated that for nonionic surfactants with a degree of ethoxylation of 25 or less, adsorption isotherms collapse to a single curve when developed in similar conditions and normalized to the CMC and maximum or plateau adsorption. Levitz et al. [11] demonstrated that isotherms could be normalized to an S-shaped isotherm for two nonionic surfactants with different alkyl chain lengths. In the normalized isotherm all three (or four) stages of adsorption are observed, which, as previously discussed, is characteristic of a surfactant with a low degree of ethoxylation. Without normalization, the adsorption isotherm of the surfactant with the shorter alkyl chain length would be

shifted to higher equilibrium concentrations as compared to the isotherm for the longer alkyl chain length; however, normalizing the adsorption isotherm with the respective CMC and maximum adsorption density results in the isotherms collapsing to a single, normalized isotherm.

Similar behavior has also been observed for surfactants with a degree of ethoxylation greater than 25; an example of this can been seen in Figure 5.[41,42] When considering normalization among adsorption isotherms, the distinction between the case of adsorption for nonionics with a low degree of ethoxylation versus the case of nonnionics with a high degree of ethoxylation is once again emphasized. In both cases, normalized adsorption isotherms collapsed to a single curve; however, a surfactant with a high degree of ethoxylation and one with a low degree of ethoxylation would not collapse to the same curve because the different size of the head groups result in a different adsorption mechanism as described earlier, with the large EO-chain of the highly ethoxylated surfactants preventing surface aggregate formation.

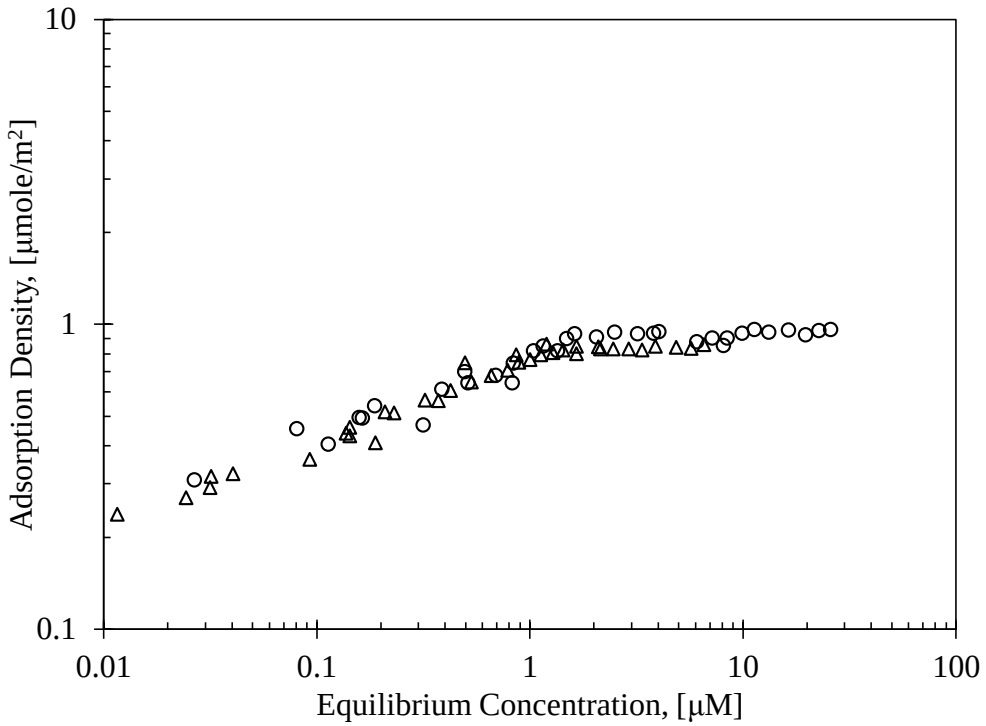

Figure 5: Normalized adsorption isotherm data for OP-40 (△), NP-40 (○) on fumed silica at 30°C.

It is clear that specific adsorption conditions including surfactant molecular structure, adsorbent, solvent, additives, and temperature have a large influence on adsorption and in some cases on the mechanism of adsorption as well as the shape of the resulting adsorption isotherm.[13,26,43] Taken together these results suggest a consistent mechanism of adsorption and a relationship between adsorption at the solid-liquid interface and bulk aggregation.[41] For nonionic surfactants of similar structure, the collapse of their adsorption isotherms when normalized using bulk aggregation properties to a single curve further proves this relation.[11,41,42] This normalization phenomena can be used as a predictive tool for determining the adsorption density of differently surfactants. If the adsorption isotherm and CMC is known for one surfactant, the adsorption isotherm for a second, similarly structured surfactant can be predicted based on the CMC. Work is being done to investigate whether changes in the

CMC due to the presence of electrolytes can aid in predicating changes in adsorption density.[42]

Characterization of Adsorbed Layer

While general observations can be drawn from the shape of the developed adsorption isotherms, probing the adsorbed surfactant layer gives further insight into the behavior of the adsorbed surfactant molecules. Several papers[15,17,20,45] have demonstrated through atomic force microscopy (AFM) that nonionic surfactants with a degree of ethoxylation of 25 or less on a hydrophilic surface form various globular structures depending on the system conditions. The work of Blom et al.[45] shows that the surfactant configuration at the surface changes from globules to rods to mesh-like within the span of 10°C. Parallels between the changing surfactant aggregation shape with increasing temperature were made between the solid/solution interface and that in the bulk solution.[45] Ellipsometry studies[21,24] have also contributed to the evidence and characterization of surface aggregates by demonstrating a predictable adsorbed layer thickness based on surfactant structure for polyethoxylated nonionic surfactants with a degree of ethoxylation of 25 or less on a hydrophilic surface. Similar results for surfactants with a high degree of ethoxylation are missing, but we hypothesize monolayer adsorption due to the large surfactant head groups sterically hindering alkyl-alkyl association. Previous ellipsometry[23,24], reflectometry[18,46], and dynamic light scattering[18] studies have shown that the thickness of the adsorbed layer for nonionic surfactants with a low degree of ethoxylation to be approximately the length of twice the surfactant's alkyl chain. Recent ex situ ellipsometry work[47] for surfactants with a high degree of ethoxylation have shown the adsorbed layer to be around 5 Å or less,

indicating monolayer formation. This monolayer would have similar characteristics to adsorbed PEG since it is the ethylene oxide units responsible for hydrogen bonding with the surface; thus, an adsorbed thickness of < 5 Å for PEG-22 is in accord with an adsorbed monolayer hypothesis.[18]

Conclusions

Evidence for parallels between surfactant assembly at the solid-liquid interface and in the bulk solution continues to grow as new methods of characterization are being applied to the solid-liquid interface. Multiple lines of evidence show conclusively that for surfactants with low degrees of ethoxylation (less than 25 EO groups) micelle-like surface aggregates form on silicon oxide surfaces at coverages as low as 0.1 monolayers. AFM images show various types of surface aggregates for surfactants with a low degree of ethoxylation. Calorimetric studies confirm that these aggregates form due to hydrophobic association between the alkyl chains, in the same manner in which hydrophobic bonding between alkyl groups also contributes to micelle formation in bulk solution. In contrast, nonionic surfactants with a high degree of ethoxylation do not form micelle-like surface aggregates. For these surfactants the strength of the hydrogen bonding between the oxygen molecules in the EO chain controls the structure of the adsorbed layer, preventing aggregation of the alkyl chains. While there is no evidence for surface aggregates for nonionic surfactants with a high degree of ethoxylation, highly ethoxylated nonionic surfactant behavior at the solid-liquid interface can still be inferred from bulk solution properties such as cloud point and critical micelle concentration and predicted by an adsorption isotherm normalized by the surfactant's CMC value. Study of the relation between the solid-liquid interface and

bulk solution has led to predictive models which can be used with relative ease in situations where surfactant adsorption must be taken into consideration.

Chapter 2: Influence of Salts on Highly Ethoxylated Nonionic Surfactants in Relation to the Hofmeister Series

Introduction

According to the U.S Energy Information Administration in 2013, there are close to 260 billion barrels of technically recoverable crude oil resources.[48] Surfactants used in enhanced oil recovery play a vital role in extraction from these reserves. A key factor in lowering extraction cost is lowering surfactant adsorption in the reservoir. Ionic surfactants are commonly used due to their ability to withstand high temperatures. However, ionic surfactants tend to precipitate in the presence of salts which creates a problem considering that salt concentration in reservoir brine can reach upwards of 300 g/L. [49] The use of highly ethoxylated nonionic surfactants can address this issue since these surfactants can maintain solubility in the presence of high salt concentrations.[39]

Despite the improved salt tolerance, nonionic surfactants are still affected by the presence of salts and the effect can be described by the Hofmeister series. The Hofmeister series classifies ions as either kosmotropic, salting in, or chaotropic, salting out, based on that ion's influence on macromolecules. An example of the Hofmeister series is shown in Figure 6.

Salting Out ---------- Salting In

$$SO_4^{2-} > HPO_4^{2-} > F^- > Cl^- > Br^- > I^- > NO_3^-$$

$$NH_4^+ > Cs^+ > Rb^+ > K^+ \approx Na^+ > H^+ > Ca^{2+} > Mg^{2+} > Al^{3+}$$

Figure 6: An example of the Hofmeister series for anions and cations arranged in increasing salting in strength.

While the exact mechanism that produces the Hofmeister phenomena is still being debated, changes in water activity due to ion presence have been successfully proven.[50]

Chaotropic ions increase water activity and are shown to have greater activity with itself than other water molecules while kosmotropic ions decrease water activity and are shown to have greater interactions with molecules other than itself.[51] One hypothesis for the Hofmeister phenomena is that the ions either increase or decrease the hydrogen bonded structure of water.[39] Structure-making kosmotropic ions are small with a high charge density. These ions induce an entropy loss in water which results in an increase in surface tension and viscosity. Structure-breaking chaotropic ions are large with a low charge density. These ions increase the system entropy by disrupting the surrounding hydrogen bound water; thus, increasing the concentration of unbound water molecules making them more available for solubilizing the macromolecule. An exception to this is polyvalent cations which tend to form complexes with ethoxylated surfactants, thereby aiding the surfactant's ability to stay in solution.

The Hofmeister phenomenon is observed as a shift in the surfactant's critical micelle concentration (CMC) when salts are present.[30] In an aqueous solution, the CMC decreases with increasing hydrophobic character of the surfactant which, for nonionic ethoxylated surfactants, would be an increase in alkyl chain length or decrease in ethylene oxide (EO) units. When kosmotropic ions are present in solution with ethoxylated nonionic surfactants, the water activity is decreased and the surfactants are not able to fully hydrate resulting in a lower CMC. Increasing the ionic concentration increases this effect until the surfactant forms a coacervate, salting out. When chaotropic ions are present in solution, nonionic surfactants remain hydrated at concentrations greater than their deionized water CMC.[30]

Adsorption isotherms for ethoxylated alkyl surfactants are well studied for surfactants with EO numbers less than 25.[8-24] For these surfactants, adsorption on a hydrophilic surface occurs due to hydrogen bonding with the surface and hydrophobic association among the alkyl tails.[8,9] This type of adsorption results in the formation of surface aggregates and a high adsorption density. The relationship between adsorption density and surfactant concentration is given in Equation 12.[13]

$$\Gamma = \frac{\Gamma_\infty K c^n}{1 + K c^n} \quad \textbf{(12)}$$

Adsorption of higher ethoxylated surfactants, greater than 25 EO units, occurs due to hydrogen bonding with the surface.[8,9,14,16,41] Because of the different mechanism of adsorption compared to lower ethoxylated nonionic surfactants, a different relationship between adsorption density and surfactant concentration is given in Equation 13.[41]

$$\Gamma = \frac{\Gamma_\infty K c^{\frac{1}{p}}}{1 + K c^{\frac{1}{p}}} \quad \textbf{(13)}$$

Further discussion on the development on this relationship is given elsewhere.[47]

An increase in adsorption density has been observed with an increase in NaCl concentration.[9,12] The presence of aqueous NaCl dehydrates the EO units of the surfactant, making adsorption at a surface more favorable than remaining in solution. The change in adsorption density occurs from the same forces that shift the CMC, leading one to believe that an increase or decrease in adsorption density can be observed based on the specific salt present.[52] This paper investigates the behavior of highly ethoxylated alkyl surfactants and salts in relation to the Hofmeister series.

Materials

Polyethoyxlated octyl and nonyl phenols were supplied by Huntsman Corporation and Stepan Company under the product name Surfonic and Makon, respectively. Table 1 provides a selected properties summary for these nonionic surfactant. All surfactants were used as received. These nonionic surfactants are polydisperse surfactants, with the distribution of ethylene oxides in the polymer chain described by a Poisson distribution. The distribution in the surfactant's ethylene oxide group results in a minimum in surface tension-concentration curves and a maximum in adsorption density-equilibrium concentration curves. The average number of ethylene oxides in the chain is given in Table 1 as the EO number. This paper refers to polyethoxylated octyl and nonyl phenols as OP-X and NP-X, respectively, where X represents the moles of ethylene oxide present in the surfactant.

Hydrophilic fumed silica with a BET surface area of 300 m^2/g and average particle size of 10 nm, Aerosil 300, was supplied by Evonik Industries and used as received.

Sodium chloride (ACS reagent, >= 99.0%), potassium chloride (ACS reagent, >=99%), calcium chloride (assay >= 99%), ammonium sulfate (assay >=99.0%) and calcium iodide (assay >=99.95%) were purchased from Sigma-Aldrich Corporation and used as received.

Table 1: Surfactant Structure

Surfactant	Company	Average Alkyl Chain Length	Average EO Number	Molecular Weight (g/mole)
Surfonic OPB-407	Huntsman	8	40	1970

Surfonic NB-557	Huntsman	9	55	2646
Surfonic NB-407	Huntsman	9	40	1980
Makon 10	Stepan	9	10	840

Methods

Adsorption Isotherms

Adsorption studies were performed by allowing 20 mL of surfactant solution of a known concentration to equilibrate with 0.3 grams of fumed silica in the presence of a fixed salt concentration. After preparation, each sample was vortexed for 1 minute, placed in a 30°C water bath and allowed to equilibrate for 24 hours. At the end of 24 hours, the equilibrium concentration was determined by UV analysis at 224 nm. The variable wavelength detector (G1314A) used is part of the Agilent 1100 series HPLC. Agilent ChemStation software was used to collect and analyze the data. The adsorption density was calculated based on the depletion of surfactant from the supernatant after the equilibration period of 24 hours. Adsorption isotherms were obtained by plotting the adsorption density versus equilibrium surfactant concentration at a fixed salt concentration.

Critical Micelle Concentration

The Wilhelmy plate method was used to measure surface tension and determine the surfactant's CMC with various salts at different salt concentrations. Measurements were taken using a Cahn dynamic contact angle analyzer (DCA-322) at room temperature, 22°C. A 20 mL solution of known surfactant concentration and fixed salt concentration was prepared for each surface tension measurement. The CMC is taken as the break in the plot of surface tension versus surfactant concentration on a log scale

from a linear decrease to a constant y-axis value. Because the surfactants in this study were not pure, there was slight increase in surface tension before constant surface tension was reached. This is due to the low solubility components of the surfactant acting at the interface below the CMC; however once the CMC is reached, these low solubility components partition into the interior of the micelle resulting in a slight increase in surface tension. For these reasons, the CMC is the minimum point in the surface tension versus concentration graph, and not when the constant surface tension is reached, as this would result in higher than actual CMC values.

Results and Discussion

Critical Micelle Concentration

The CMC results are in Figure 7, Figure 8, and Table 2. The absence of a local minimum in Figure 7 demonstrates the purity of the NP-10 surfactant. The local minimums in Figure 8 are a result of low solubility components in the surfactant. In this situation, the CMC is taken as the local minimum. The minimum occurs due to surfactant's low solubility components interacting with the air/water interface. Once the CMC occurs, these low solubility components leave the air/water interface and partition into the micelles eventually resulting in a constant surface tension. Comparing the three highly ethoxylated nonionic surfactants, OP-40 is the most hydrophilic because it has one less carbon than NP-40 and NP-55. The addition of a carbon on the alkyl chain decreases the CMC more than the addition of an ethylene oxide unit increases the CMC. This agrees with literature stating that the CMC will double with the addition of 12 EO units yet the depletion of only one methylene group is required for this same change.[26]

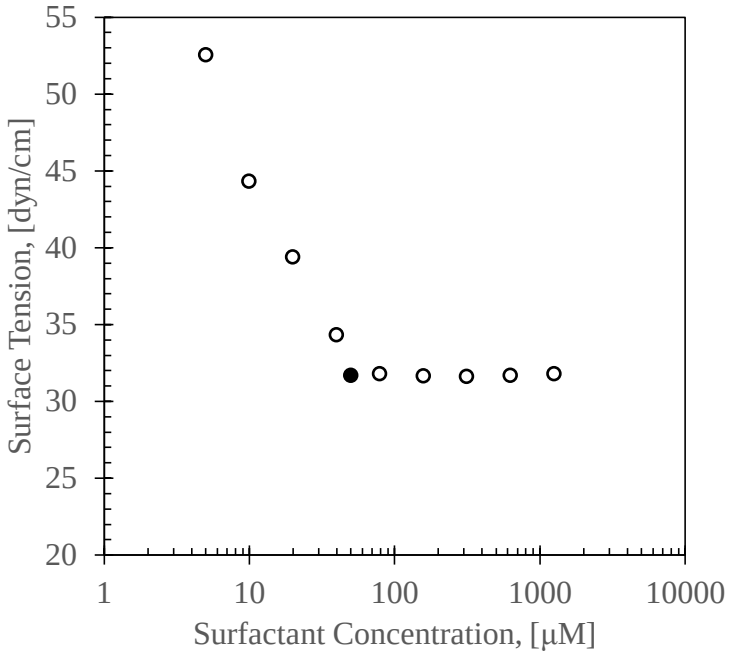

Figure 7: Surface tension versus surfactant concentration in deionized water for NP-10. CMC = 50.1 μM (●)

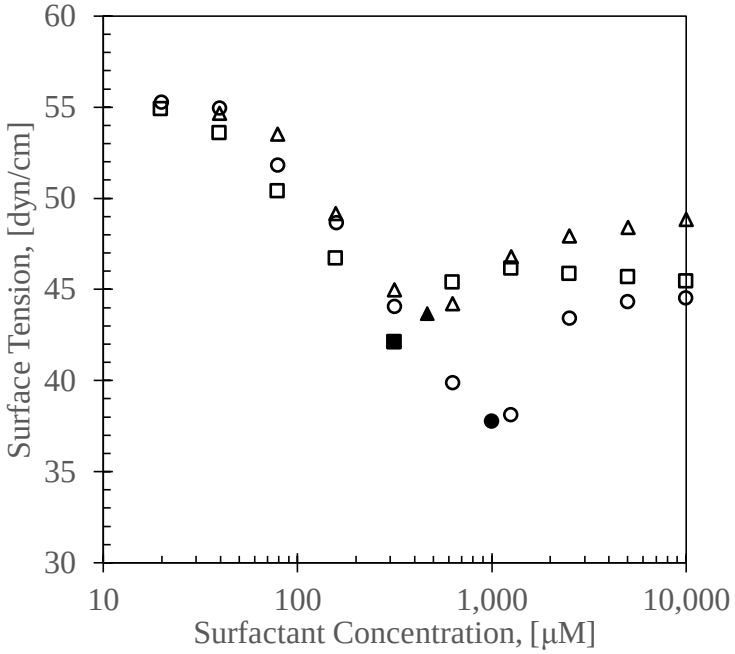

Figure 8: Surface tension versus surfactant concentration in deionized water for OP-40 (○), NP-40 (□), and NP-55 (△). OP-40, CMC = 1000 μM (●); NP-40, CMC = 315 μM (■); NP-55, CMC = 465 μM (▲)

Table 2: Critical micelle concentration for polyethoxylated alkyl phenols at 25°C in the presence of various salts and salt concentrations.

	NP-10	OP-40	NP-40	NP-55
	[μM]			
DI Water	50.1 ± 0.9	1000 ± 7	315 ± 2	465
0.6 M NaCl	35.6 ± 0.1	531	191	375 ± 5
1.5 M NaCl	19.0 ± 0.4	279	114 ± 5	126 ± 1
1.5 M $CaCl_2$	-	369 ± 2	151	228
1.5 M KCl	-	338 ± 2	130	145 ± 3
0.6M $(NH_4)_2SO_4$	-	222	61.4 ± 1	123 ± 2

In Table 2, the highest CMC values among the surfactants occur in deionized water because all the salts listed are composed of two kosmotropic ions with the exception of $CaCl_2$. Increasing the concentration of kosmotropic ions dehydrates the ethylene oxide groups making the surfactant more hydrophobic and decreasing the CMC. The large difference in the CMC between OP-40 and NP-40 in deionized water is minimized in the presence of NaCl which implies that the surfactants have a high sensitivity to the presence of kosmotropic ions. The CMC values are greater for $CaCl_2$ compared to NaCl and KCl because the calcium ion has a chaotropic effect which makes up for twice the chlorine ions present. The salt that had the greatest salting out effect was $(NH_4)_2SO_4$. Even though this salt was only present at 0.6 M, it is composed of two strongly kosmotropic salts which resulted in the lowest measured CMC values.

Adsorption Isotherms with No Salts Present

Adsorption isotherms in deionized water at 30°C for the four nonionic surfactants used in this study are shown in Figure 9. The adsorption density for NP-10 is the highest among the four surfactants due to its ethylene oxide head group allowing the formation of surface aggregates. It is clear that the longer ethylene oxide chains hinder the formation of surface aggregates for the other three surfactants because the

adsorption density is less than half compared to NP-10. The slope of adsorption is higher for NP-10 due to the added attractive hydrophobic forces of the alkyl tails in addition to the hydrogen bonding between the ethylene oxide head groups and the oxidized silica surface. Additionally, adsorption at the surface does not become hindered by a smaller NP-10 molecule until surfactant concentration is near the CMC, while a larger NP-55 molecule occupies more surface area and adsorption appears to be hindered even a lower concentrations.

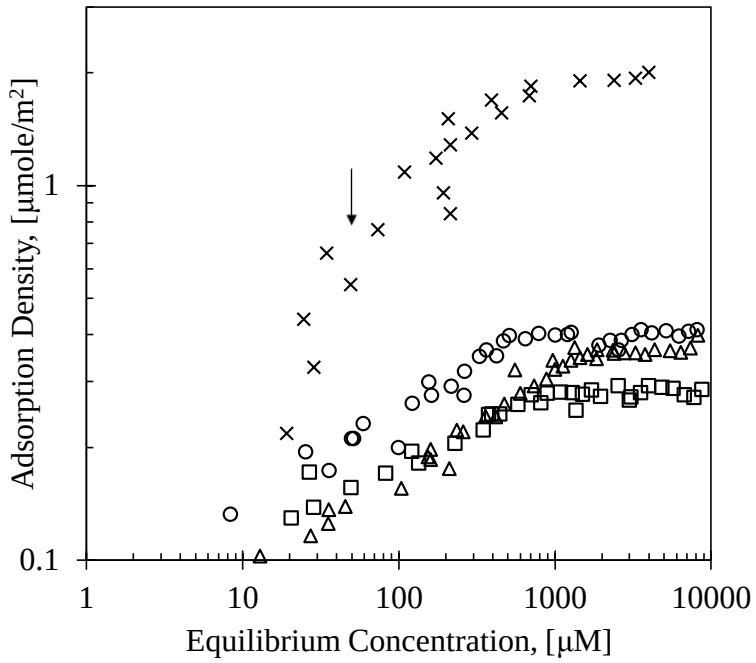

Figure 9: Adsorption isotherms for OP-40 (△), NP-40 (○), NP-55 (□), NP-10 (x) developed at 30°C in deionized water with fumed silica. CMC of NP-10 marked with arrow.

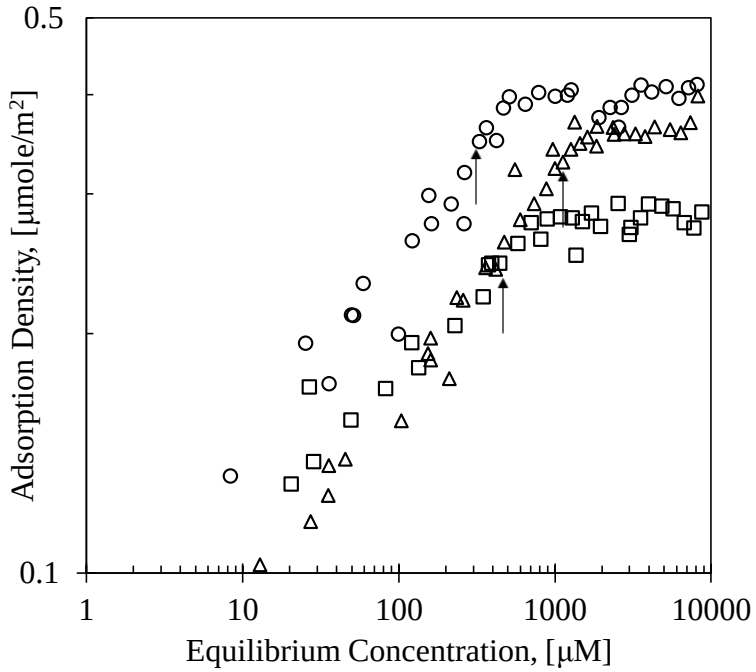

Figure 10: Adsorption isotherms for various nonionic ethoxylated surfactants developed at 30°C in deionized water with fumed silica, focusing on a degree of ethoxylation of 40 or greater. OP-40 (△), NP-40 (○), NP-55 (□). CMCs marked with arrow.

Figure 10 focuses on the adsorption isotherms for the nonionic surfactants with the larger head groups. The decrease in adsorption density of NP-55 compared to NP-40 and OP-40 is due to the slightly larger ethylene oxide head group occupying more surface area on the silica. When comparing the adsorption isotherms of NP-40 and OP-40, the plateau onset occurs at a lower concentration for NP-40 because of the surfactant's lower CMC due to its longer hydrophobic chain. The slope of adsorption between OP-40 and NP-40 is the same due to the surfactant's identical head structure. The slope of adsorption of NP-55 is lower in comparison due to the surfactant's larger head group.

These results agree with the literature that the adsorption density for nonionic surfactants on a hydrophilic surface depends on the head group size and that there is a

different mechanism of adsorption for nonionic surfactants with a smaller versus a larger head group.

Adsorption Isotherms with 1.5 M NaCl, KCl, $CaCl_2$ Present

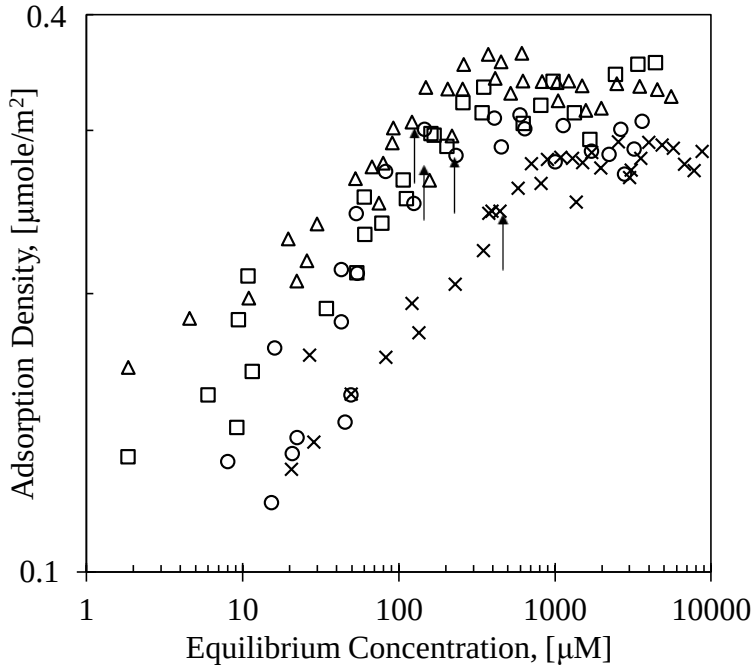

Figure 11: Comparisons of adsorption isotherms for NP-55 with 0 M salt (x), 1.5 M NaCl (△), 1.5 M $CaCl_2$ (○), and 1.5 M KCl (□). CMCs marked with arrow.

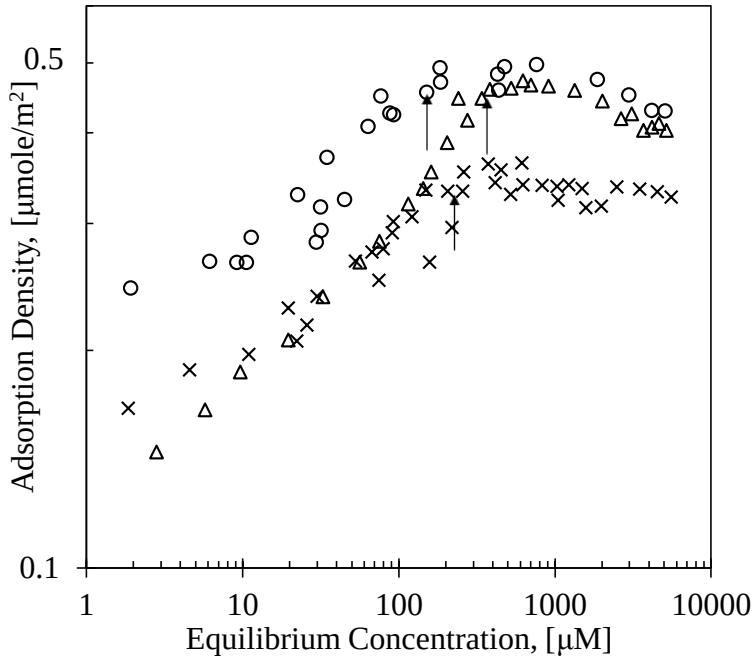

Figure 12: Adsorption isotherms for various nonionic ethoxylated surfactants developed at 30°C with 1.5 M NaCl and fumed silica. OP-40 (△), NP-40 (○), NP-55 (x). CMCs marked with arrow.

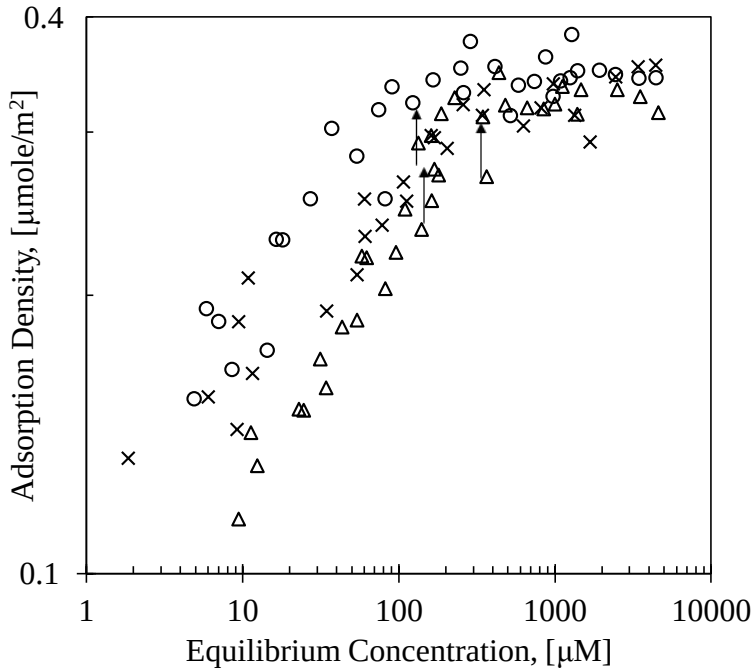

Figure 13: Adsorption isotherms for various nonionic ethoxylated surfactants developed at 30°C with 1.5 M KCl and fumed silica. OP-40 (△), NP-40 (○), NP-55 (x). CMCs marked with arrow.

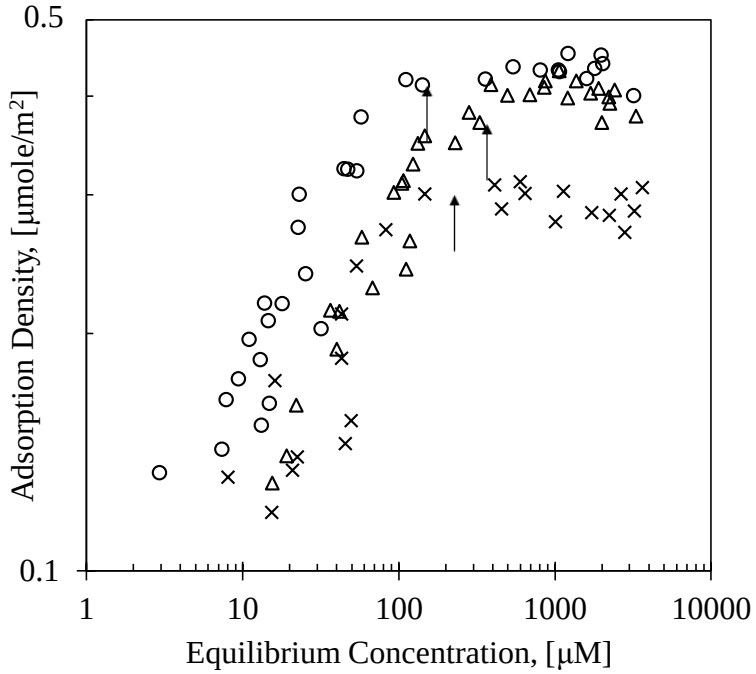

Figure 14: Adsorption isotherms for various nonionic ethoxylated surfactants developed at 30°C with 1.5 M $CaCl_2$ and fumed silica. OP-40 (Δ), NP-40 (○), NP-55 (x). CMCs marked with arrow.

Adsorption isotherms were developed in the presence of 1.5 M NaCl, KCl, and $CaCl_2$ for the OP-40, NP-40, and NP-55. Adsorption density increased in the presence of these salts while the slope of adsorption was unchanged. A comparison of adsorption isotherms for NP-55 in the presence and absence of the salts is presented in Figure 11. In addition to the increase in adsorption density in the presence of these three salts, the CMC shifts to a lower concentration. The adsorption isotherm shift created by the presence of NaCl and KCl is similar and in agreement with the Hofmeister series. The sodium, potassium, and chlorides are located in the middle of the Hofmeister series, on the weaker end of the kosmotropic, salting out, ions which is why the adsorption density has only slightly increased in the presence of these salts. Sodium and potassium are located next to each other with some sources stating an equal salting out effect between the two ions which is in agreement with the data in Figure 11 showing a negligible

difference between the two developed isotherms.[53] Despite twice the concentration of the chloride in in $CaCl_2$, the adsorption density is slightly less than that of NaCl and KCl because the calcium ion has a chaotropic, salting in effect. Overall, these trends were observed for each of the highly ethoxylated nonionic surfactants.

The presence of 1.5 M NaCl, KCl, and $CaCl_2$ increased the adsorption density for the nonionic surfactants as seen in Figure 12, Figure 13, and Figure 14 but the general shape of the isotherm is unchanged when compared to no salt present in Figure 10. Based on the proposed mechanism for this adsorption process, the increase in adsorption density is either due to the salt's interaction with the surface sites and making more surface sites available, the salt is affecting the surfactant's conformation at the surface, or a combination of the two. Since the salt's influence is apparent from the shift in the surfactant's plateau, the salt influencing the surfactant solubility is most likely the case.

Adsorption Isotherms with 0.6 M NaCl, $(NH_4)_2SO_4$, and CaI_2 Present

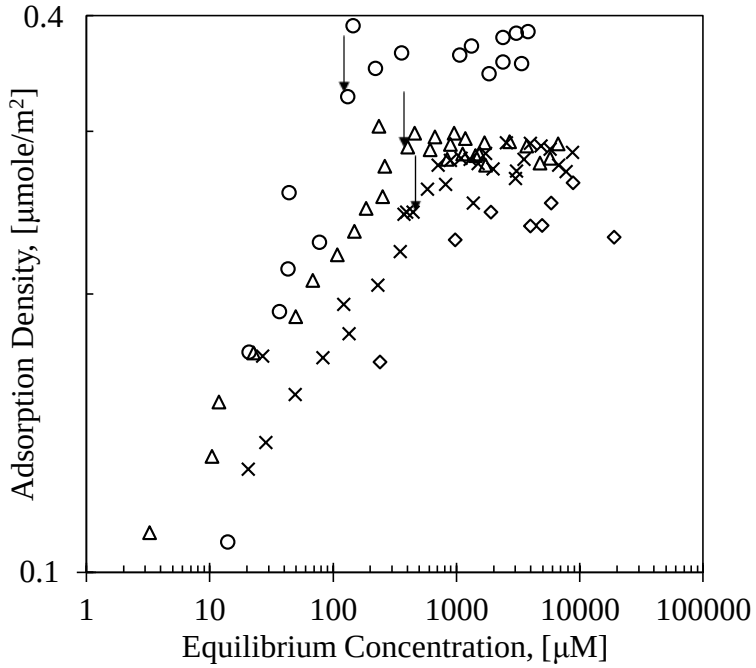

Figure 15: Comparisons of adsorption isotherms for NP-55 with 0 M salt (x), 0.6 M NaCl (△), 0.6 M $(NH_4)_2SO_4$ (○), and 0.6 M CaI_2 (◇).CMCs marked with arrow.

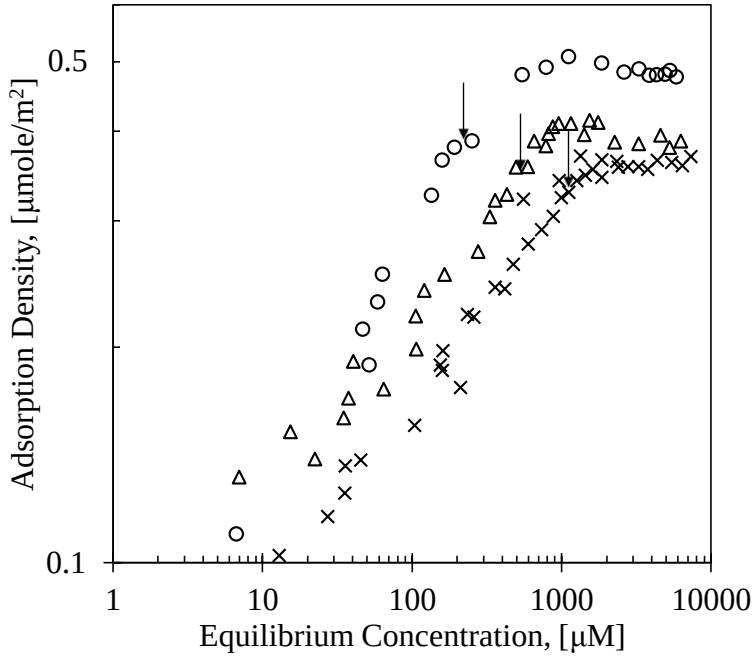

Figure 16: Comparisons of adsorption isotherms for OP-40 with 0 M salt (x), 0.6 M NaCl (△), 0.6 M NH_4SO_4 (○).CMCs marked with arrow.

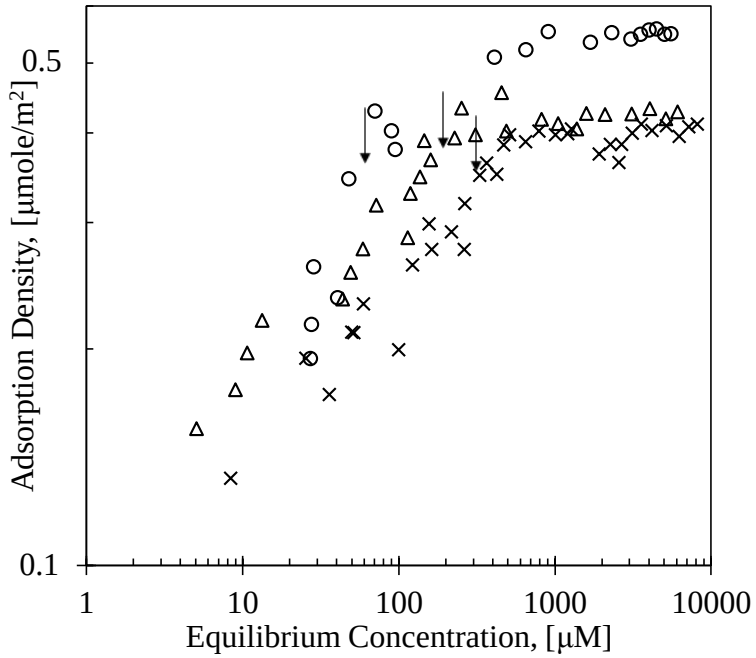

Figure 17: Comparisons of adsorption isotherms for NP-40 with 0 M salt (x), 0.6 M NaCl (△), 0.6 M $(NH_4)_2SO_4$ (○). CMCs marked with arrow.

Adsorption isotherms were developed in the presence of 0.6 M NaCl, $(NH_4)_2SO_4$, and CaI_2 for NP-55 in Figure 15, and 0.6 M NaCl and 0.6 M $(NH_4)_2SO_4$ for OP-40 and NP-40 in Figure 16 and Figure 17. In the presence of 0.6 M NaCl, the increase in adsorption density and shift in the CMC is not as apparent compared to the presence of 1.5 M NaCl due to fewer kosmotropic ions present in solution. In the presence of 0.6 M $(NH_4)_2SO_4$, the salting out effect is more dramatic compared to NaCl as both the adsorption density and slope of adsorption increase. This result agrees with the Hofmeister series that classifies both NH_4^+ and SO_4^{2-} as strong kosmotropic ions. The experiment was performed at 0.6 M $(NH_4)_2SO_4$ because at 1.5 M $(NH_4)_2SO_4$ the cloud point was lower than 30°C which further demonstrates the kosmotropic traits of these ions. Ammonium sulfate was the only salt analyzed that had an effect on the slope of adsorption. The increase in adsorption slope can be contributed to the kosmotropic nature of the ions pushing the surfactant to the interfaces, either air/water

or water/solid. With the surfactant pushed to the water/solid interface by its reduced water solubility, it is more readily available to hydrogen bond with the hydrophilic surface resulting in an increase in the slope of adsorption. The presence of calcium iodide decreases the adsorption density which agrees with the Hofmeister series as both ions are strongly chaotropic. The presence of the chaotropic ions create a salting in effect which increases their affinity for the water molecules and makes partitioning to interfaces less favorable.

Conclusions

This work demonstrates how adsorption density of nonionic ethoxylated surfactants is affect by the presence of salts and how this effect varies depending on the type of salt present. Different shifts in the critical micelle concentration are also observed with the presence of different salts. This suggests that the same hydrophilic-hydrophobic forces which control micelle formation also play a role in surfactant adsorption to a hydrophilic surface. While the adsorption density varies depending on the type of salt present, the slope of the adsorption isotherms does not vary, except for ammonium sulfate. This suggests that the salt's influence does not interfere with the mechanism of adsorption but instead with the mono- or bilayer formation of the surfactant on the hydrophilic surface.

Chapter 3: Behavior of Ionic and Nonionic Surfactants in Fracturing Matrix at High Salinity and High Temperature Conditions

Introduction

Chemical additives aid in making hydraulic fracturing more cost and time effective in the recovery of natural gas and oil. A friction reducer will reduce the pressure drop of water flowing through pipes; a biocide will help control the growth of microbes; a surfactant will reduce interfacial tension and improve wetting; a gelling agent will help carry proppant deep into the fracture; a scale inhibitor prevents mineral scale precipitates. However, there are questions as to whether these chemicals are able to effectively travel downhole, whether the chemicals become trapped in the fractured formation, or whether the chemicals travel through the rock matrix to an unintended location, such as water reservoirs.[54] There must be a thorough understanding of how these chemicals behave at reservoir conditions, temperatures of 160°C and higher[55] with up to 20% or higher TDS[56], in order to gain the full benefit of these chemicals and minimized risk.

Surfactants in fracturing fluids can undergo phase changes when placed under petroleum reservoir conditions and this paper investigates whether these changes affect the surfactants' migration through a fractured rock matrix. When nonionic surfactants reach their cloud point, the surfactant solution will separate into two phases, a surfactant enriched phase known as a coacervate and a surfactant poor phase.[32,52] Nonionic surfactant migration may also be affected by the presence of certain salt ions which can lower the cloud point and increase adsorption density.[42] According to the Hofmeister

series, when kosmotropic ions are present, adsorption density increases since these salts make the surfactant less soluble in water.[30,38]

For ionic surfactants, hindered migration through a rock matrix can be caused by the high adsorption of the surfactant onto an oppositely charged surface. Increased adsorption on similarly charged surfaces is also observed in the presence of salts because of a decrease of electrostatic repulsion.[32]

Many studies examine static and dynamic adsorption of surfactants onto different surfaces such as kaolinite[57], and Berea sand[58-60], Indiana limestone[60], and Lock Port dolomite[60]. However, these studies lack a focus on high temperature and high salinity conditions. The highest salt concentration reported was 2 wt% salt[58,60] and the highest temperature was at 90°C[58]. Additionally, it is important to consider the combined effect of salinity and temperature. For example, with nonionic surfactants, an increase in salinity increases surfactant adsorption and decreases the surfactant's cloud point temperature, both of which have the potential to effect the surfactant's migration through a formation. This study focuses on how the migration behavior of ionic and nonionic surfactants is affected by the high salinity and high temperature conditions.

Materials

Shale samples were obtained from the Oklahoma Geological Survey and the Pennsylvania Department of Conservation and Natural Resources. The received samples were ground and sieved. The shale collected between 150 to 250 microns was used. BET measurements showed the Marcellus shale to be 39.4 m^2/g

Ottawa sand was received from U.S. Silica Company with an approximate particle size between 100-200 microns. BET measurements showed the Ottawa sand to be 0.0438 m^2/g.

A polyethoxylated alkylphenol nonionic surfactant supplied by Huntsman Chemical was used in this study. The nonionic surfactant is a polydisperse surfactant with a Poisson distribution of ethylene oxides in the polymer chain; it has an alkyl chain length of 9, with 55 ethoxy units, and a molecular weight of 2646. This surfactant will be referred to as NP-55. In deionized water, NP-55 has a cloud point around 105°C.

Sodium dodecylbenzene sulfonate (SDBS) was supplied by Stepan Company and was used as received. The surfactant is soluble in deionized water, but insoluble in the presence of 10 wt% sodium chloride.

A branched C12 sodium diphenyl oxide disulfonate (DPDS) was supplied by Pilot Chemical Company. The surfactant was used as received. The surfactant was tested with 0 to 20 wt% NaCl and remained soluble.

Methods

A metal column (250 mm x 9 mm ID) fitted with 60 micron inlet and outlet filters is packed with shale, proppant, or 1 mm glass beads. The column is connected to a syringe pump (Teledyne Isco D-Series) with a 300 mL accumulator. All connections are made with 1.5 mm-OD metal tubing. At 0.03 mL/minute, fracturing fluid flows from the accumulator to a 40 micron particle filter before entering a convection oven (Yamato DKN 402). Once in the convection oven, the fluid flows through the 60 micron pre-filter, followed by the packed metal column, and finally the 60 micron post-filter. The oven temperature ranges from 30 to 150°C depending on the experimental

run. The fracturing fluid exits the convection oven and flows to a room temperature water bath before meeting with a 90 PSI back pressure regulator. After this, the fluid openly flows into a graduated burette for sample collection. A schematic of this set up is given in Figure 18.

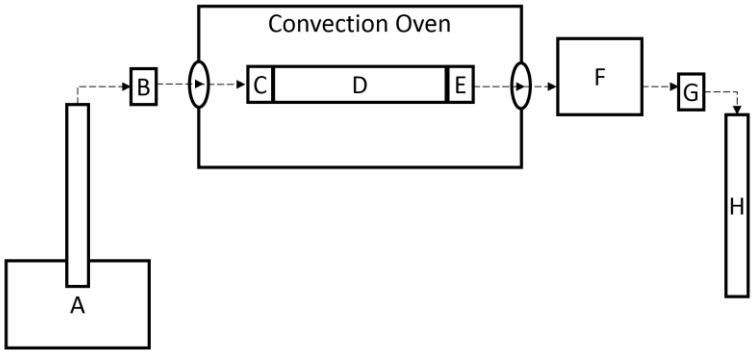

Figure 18: Schematic of fluid flow from pump and accumulator (A) to 40 μm filter (B) into the convection oven to the 60 μm pre-filter (C) to the filled steel column (D) to the 60 μm post-filter (E) to the room temperature water bath (F) to the back pressure regulator (G) to the graduated burette (H). Fluid flow is represented by the dashed arrow.

The fracturing fluid contains between 0-20% by weight sodium chloride and 0-1% by weight surfactant. Samples are collected and analyzed to determine the TDS and weight percent of surfactant still remaining in solution.

Once the equipment was set up, deionized water was run through the system at 0.03 mL/minute at varying temperatures, usually 30, 100 and 150°C, for approximately 5 sand/shale pack pore volumes at each temperature, though longer time was spent at the initial temperature to check that there were no leaks or plugs in the system. The temperature gradient with deionized water was performed to ensure no excess salt was coming off the ground shale samples. This methodology was continued with other non-shale samples for continuity among runs. Simulated fracturing fluid containing surfactant and possibly sodium chloride was then run through the system at 0.03

mL/minute and at varying temperatures, 90, 100, 110, and 120°C, for approximately 5 pore volumes at each temperature. This was followed by deionized water at room temperature for approximately 30 pore volumes.

A high performance liquid chromatograph (HPLC), Agilent 1100 series, was used to determine the concentrations of all surfactants used before and after contact with the shale, proppant, or glass beads. The HPLC set up included the following equipment: G1312A Binary Pump, G1313A Autosampler, G1316A Thermostatted Column Compartment, G1379 Microdegasser, and a G1314A Variable Wavelength Detector.

HPLC samples were filtered before analysis with a 20 micron syringe filter. Samples were run through a Waters C18 reverse phase chromatography column. The carrier solvent used in analysis was a combination of HPLC grade acetonitrile and HPLC grade water purchased from Pharmco Aaper. The ratio of organic to aqueous phase carrier solvent was varied over time to separate any remaining TDS from the surfactants. Data was collected and analyzed using Agilent's ChemStation.

Disposable aluminum weighing boats were used to determine a collected sample's TDS. The aluminum boats were weighed empty and then re-weighed with the fracturing fluid. The fracturing fluid in the aluminum boat was allowed to evaporate overnight in a 90°C convection oven. The dried boats were re-weighed the following morning. The difference between the dried and the aluminum boat itself was taken as the TDS per fracturing fluid weight.

Results and Discussion

When analyzing the results for nonionic surfactant NP-55 in Figure 19 through Figure 24 , it is important to note the different fluid behavior below and above the cloud point of NP-55 which is 105°C in deionized water and 85°C with 10 wt% NaCl. Below the cloud point, surfactant concentration exiting the column is less than the initial 1 wt% surfactant injected. This concentration drop at the exit of the column results from surfactant adsorption within the column. After this drop, adsorption on the solid surface becomes less favorable and the surfactant effluent concentration increases until it equals the inlet concentration. When the cloud point is reached, little to no surfactant is observed exiting the column. The lack of surfactant exiting the column is due to the surfactant solution phase-separating into a surfactant-rich phase known as a coacervate and a surfactant-poor phase. The denser, surfactant-rich coacervate phase tends to have a higher viscosity that the injected surfactant solution, and may even have a gel-like consistency; consequently, it does not flow as easily through the column when compared to the less dense, surfactant-poor phase. This difference in flow behavior results in the column effluent not containing any of the injected nonionic surfactant when the column temperature exceeds the cloud point of the nonionic surfactant.

After the surfactant injection, if the sand pack temperature returns below NP-55's cloud point and deionized water is pumped through the column, a high concentration of NP-55 exits the column. This high concentration exiting the column further indicates that the surfactant did not propagate through the sand pack when the temperature was above the cloud point and shows that the surfactant can still be recovered once the system drops below the cloud point temperature. It should be

emphasized that the large amount of NP-55 exiting the column in Figure 19 through Figure 22 is not only due to the system dropping below the cloud point but also to flushing with deionized water. Below the cloud point, the coacervate phase goes back into the solution and the deionized water flush allows the surfactant to desorb, as the adsorption process for these ethoxylated nonionic surfactants is reversible. In Figure 24, about 135 mg NP-55/g Woodford shale remained in the column because a deionized water flush was not performed. When the system temperature was dropped below the cloud point, a little less than half of the injected surfactant was recovered during the subsequent DI water flush.

When surfactant injection began in Figure 20 and Figure 22, the system was already above the cloud point temperature and thus NP-55 did not exit the column at any time during the surfactant injection sequence. When the system temperature returned below the cloud point temperature to 30°C and deionized water was pumped through the column, a high weight percent of NP-55 exited the column. As stated previously, this high surfactant concentration was attributed to NP-55 accumulating in the column at temperatures above the cloud point. Once below the cloud point temperature, NP-55 no longer remained in the denser, coacervate phase and was allowed to flow through the column.

The spike in surfactant concentration exiting the column in Figure 23, observed around 180 pore volumes, shows that the coacervate phase is not adsorbed to the column material, but instead moves very slowly within the column. Figure 23 demonstrates how easily a coacervate phase becomes trapped in fracturing material. Above the cloud point in Figure 23, the estimated square angstroms per surfactant

molecule, if all the surfactant was adsorbed, based on the available surface area of the solid, was less than 0.02 $Å^2$/molecule at the solid-liquid interface. This number is unrealistic as other studies have shown a surfactant molecule of this size occupies between 550 to 600 $Å^2$/molecule on a silica surface. [61,62] The experiment shown in Figure 23 was stopped before a deionized water flush was performed because of a blockage in the system, which was most likely caused by the buildup of surfactant. All of this further emphasizes that above the cloud point, the surfactant does not adsorb but instead phase separates into a nearly immobile surfactant-rich phase.

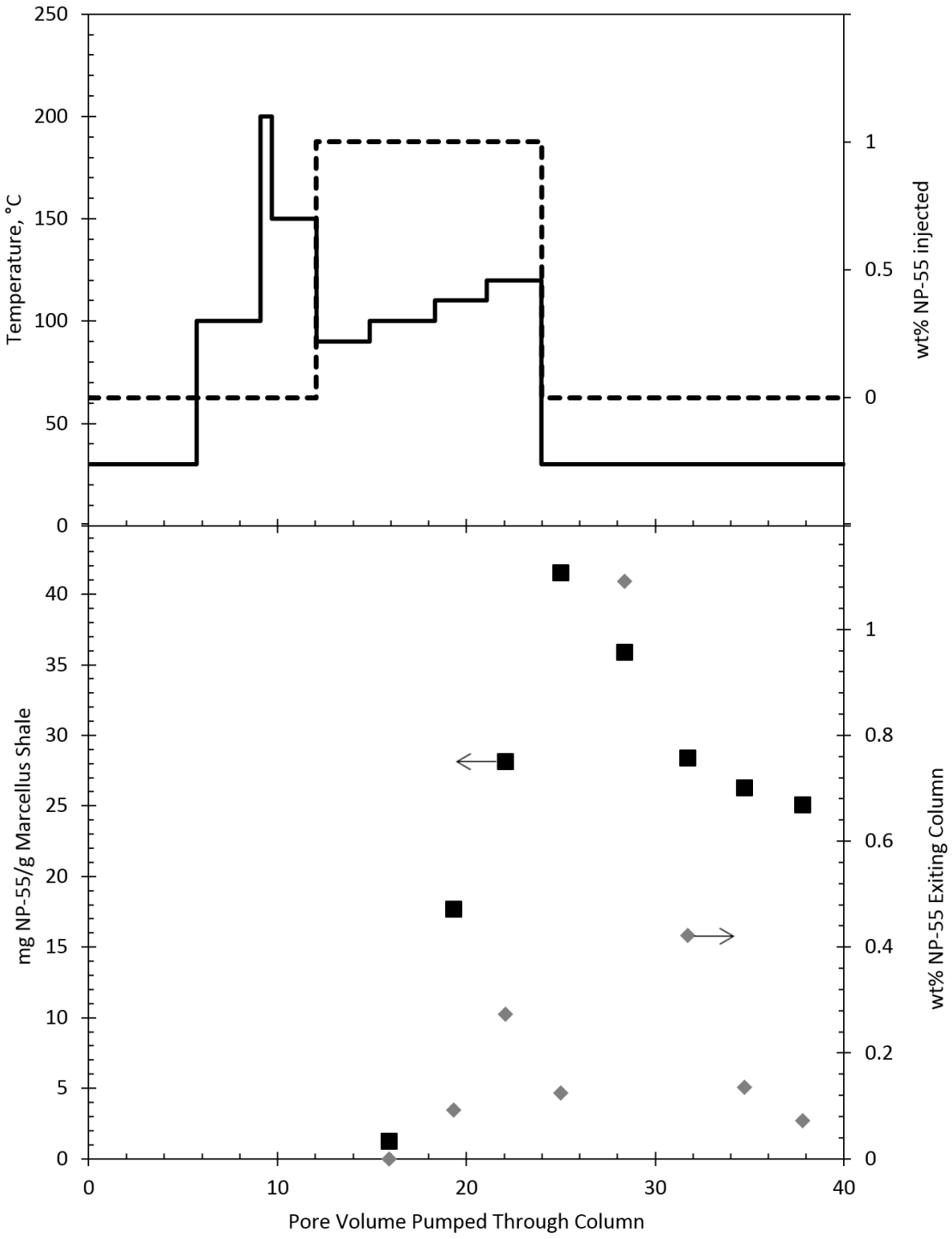

Figure 19: Experimental results from column filled with Marcellus shale and fracturing fluid of deionized water with 1 wt% NP-55. The top graph is the temperature of column (—) and wt% NP-55 injected (---) versus pore volume pumped through column. The bottom graph is wt% NP-55 exiting column (♦) and mg NP-55 adsorbed/g Marcellus shale (■) versus pore volume injected. Arrows indicate which axis to read.

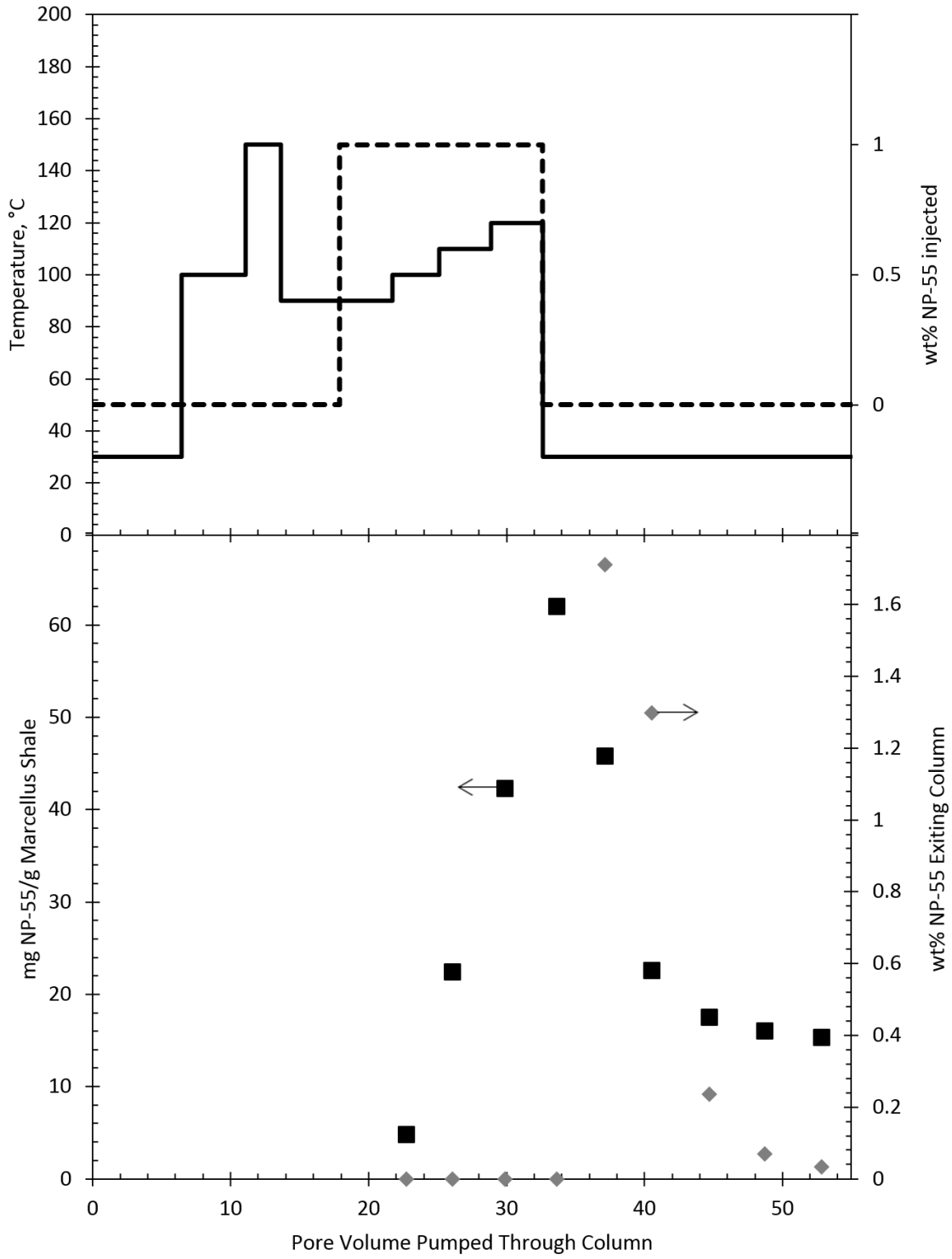

Figure 20: Experimental results from column filled with Marcellus shale and fracturing fluid with 1 wt% NP-55 and 10 wt% NaCl. The top graph is the temperature of column (—) and wt% NP-55 injected (---) versus pore volume pumped through column. The bottom graph is wt% NP-55 exiting column (♦) and mg NP-55 adsorbed/g Marcellus shale (■) versus pore volume injected. Arrows indicate which axis to read.

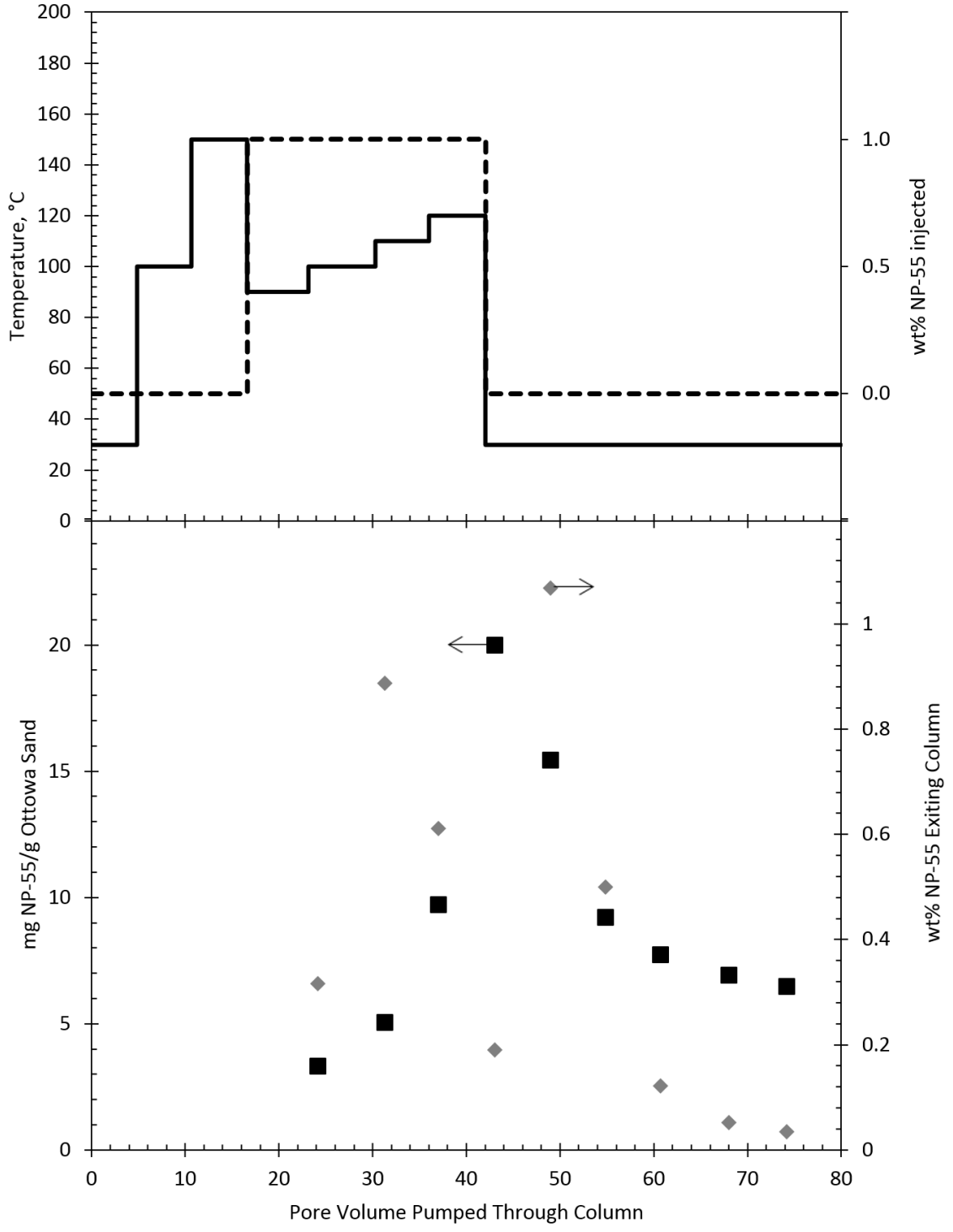

Figure 21: Experimental results from column filled with Ottawa sand and fracturing fluid of deionized water with 1 wt% NP-55. The top graph is the temperature of column (—) and wt% NP-55 injected (---) versus pore volume pumped through column. The bottom graph is wt% NP-55 exiting column (♦) and mg NP-55 adsorbed/g Ottawa sand (■) versus pore volume injected. Arrows indicate which axis to read.

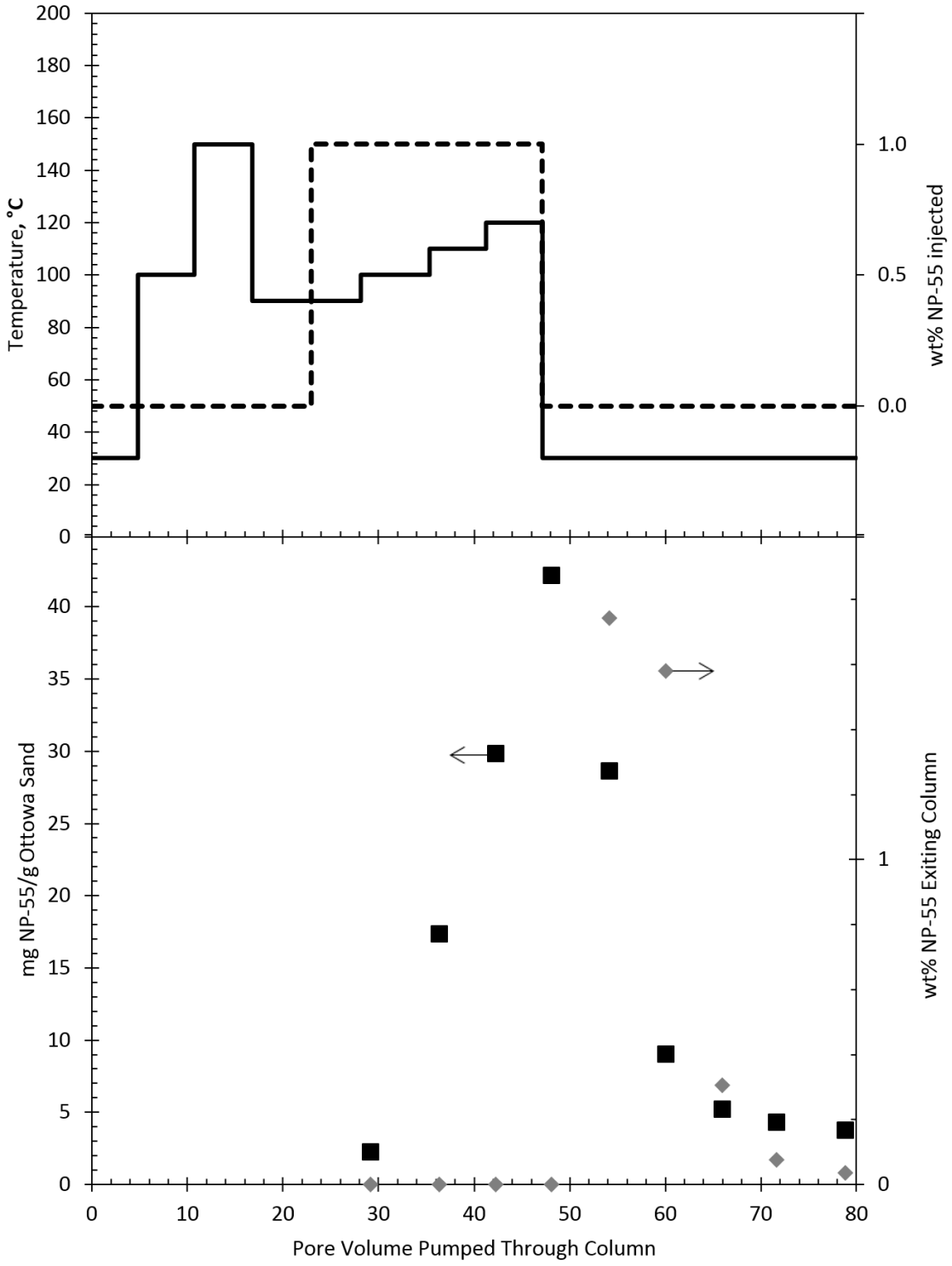

Figure 22: Experimental results from column filled with Ottawa sand and fracturing fluid with 1 wt% NP-55 and 10 wt% NaCl. The top graph is the temperature of column (—) and wt% NP-55 injected (---) versus pore volume pumped through column. The bottom graph is wt% NP-55 exiting column (♦) and mg NP-55 adsorbed/g Ottawa sand (■) versus pore volume injected. Arrows indicate which axis to read.

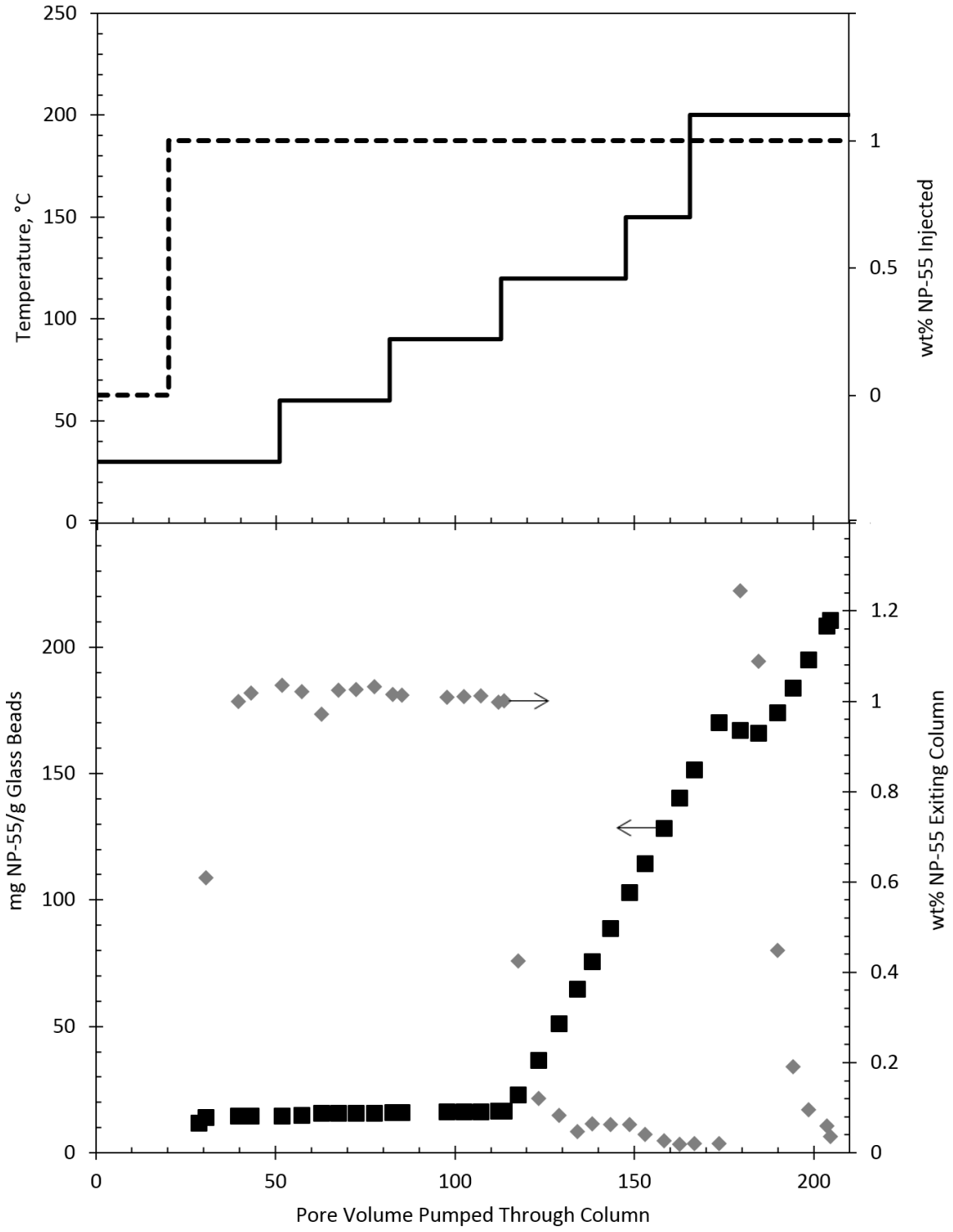

Figure 23: Experimental results from column filled with glass beads and fracturing fluid of deionized water with 1 wt% NP-55. The top graph is the temperature of column (—) and wt% NP-55 injected (---) versus pore volume pumped through column. The bottom graph is wt% NP-55 exiting column (♦) and mg NP-55 adsorbed/g glass beads (■) versus pore volume injected. Arrows indicate which axis to read.

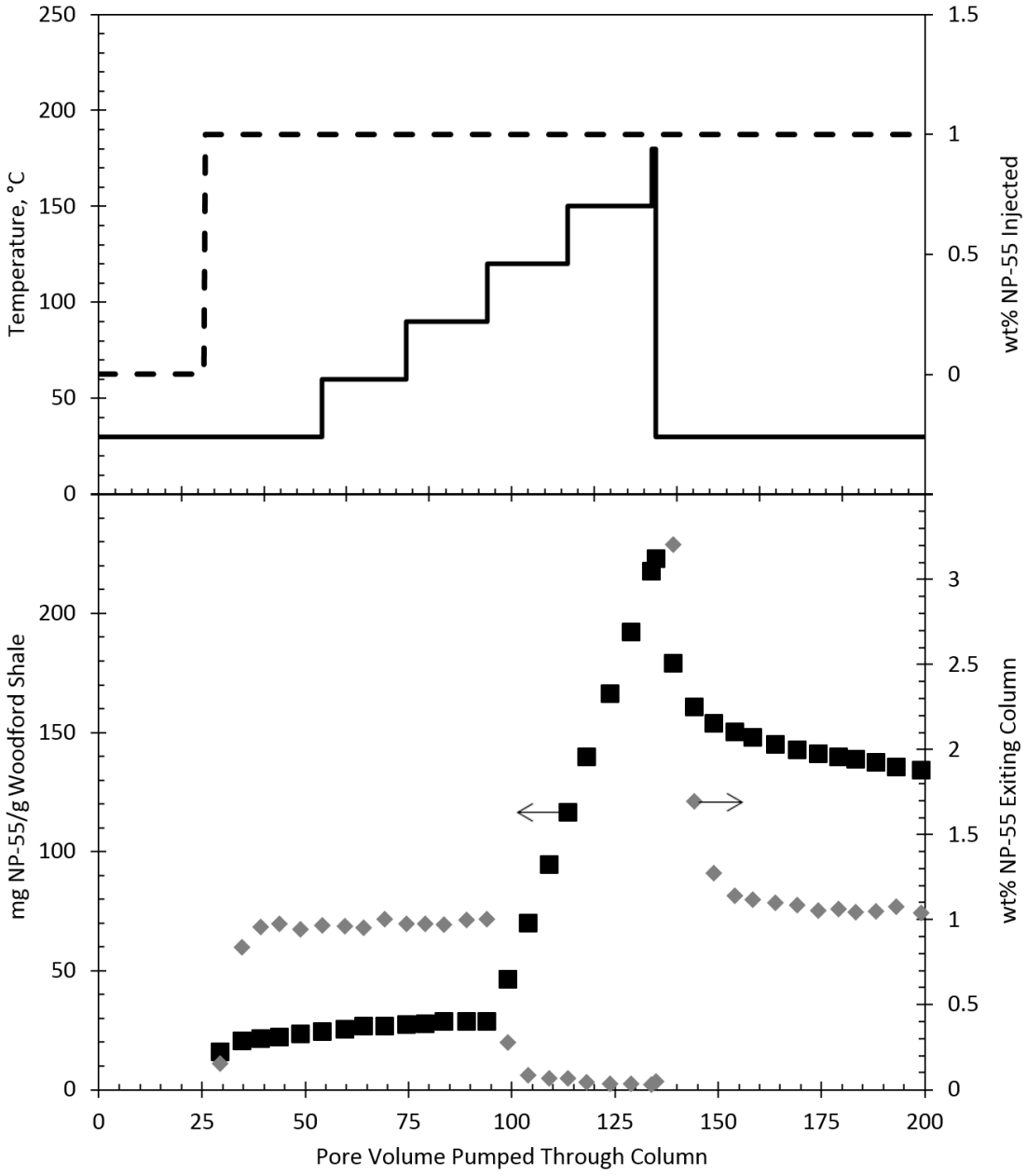

Figure 24: Experimental results from column filled with Woodford shale and fracturing fluid of deionized water with 1 wt% NP-55. The top graph is the temperature of column (—) and wt% NP-55 injected (---) versus pore volume pumped through column. The bottom graph is wt% NP-55 exiting column (♦) and mg NP-55 adsorbed/g Woodford shale (■) versus pore volume injected. Arrows indicate which axis to read.

Figure 25 and Figure 26 show the results of injecting 1 wt% sodium dodecyl benzene sulfonate (SDBS) into a column filled with Marcellus shale or Ottawa sand at

various temperatures. Regardless of the adsorbent in the column or the temperature of the system, SDBS adsorbs on the surface until maximum surface coverage is reached. In comparison with the NP-55 experiments, SDBS is not affected by high temperatures. Once deionized water is inejcted, a small amount but not all of the SDBS is observed exiting the column. This is due to the adsorbed surfactant on the solid surface re-estabilishing equilibrium with the bulk fluid. Adsorption of SDBS on a silica surface, such as the Ottawa sand and Marcellus shale, is due to a dispersion force between SDBS's benzene ring and the silanol groups on the silica surface which overcomes the electrostatic repuslion between the surfactant and the solid surface, as well as the formation of admicelles, which contain counterions.[63,64]

Experiments were only run for SDBS in deionized water since SDBS was not soluble in the presence of 10 wt% NaCl. While SDBS was more robust than NP-55 at high temperatures, injection conditions similar to deionized water is unrealistic, because of its sensitivity to dissolved salts, making SDBS unsuitable for use in enhanced oil recovery or fracturing fluids.

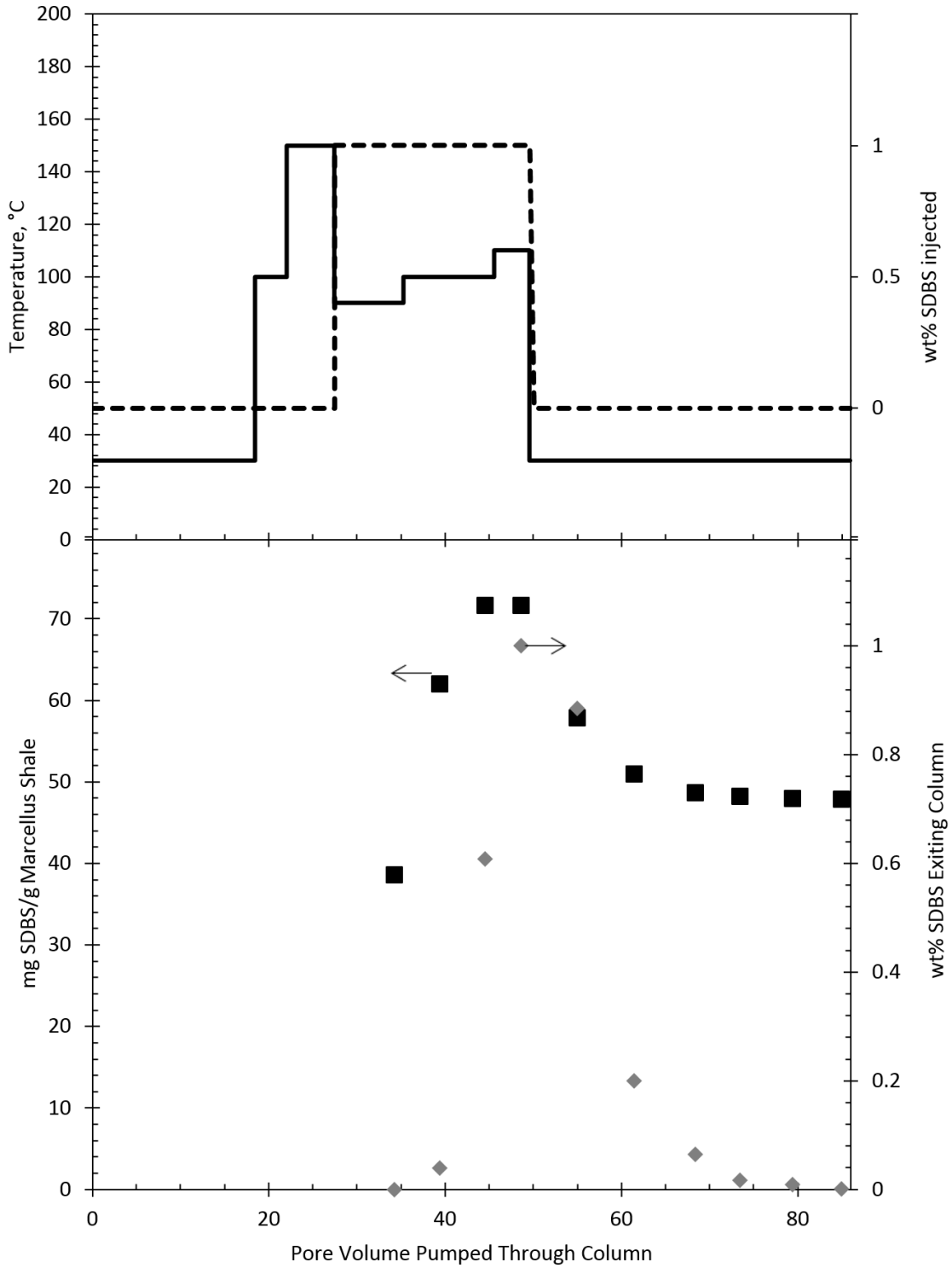

Figure 25: Experimental results from column filled with Marcellus shale and fracturing fluid of deionized water with 1 wt% SDBS. The top graph is the temperature of column (—) and wt% SDBS injected (---) versus pore volume pumped through column. The bottom graph is wt% SDBS exiting column (♦) and mg SDBS adsorbed/g Marcellus shale (■) versus pore volume injected. Arrows indicate which axis to read.

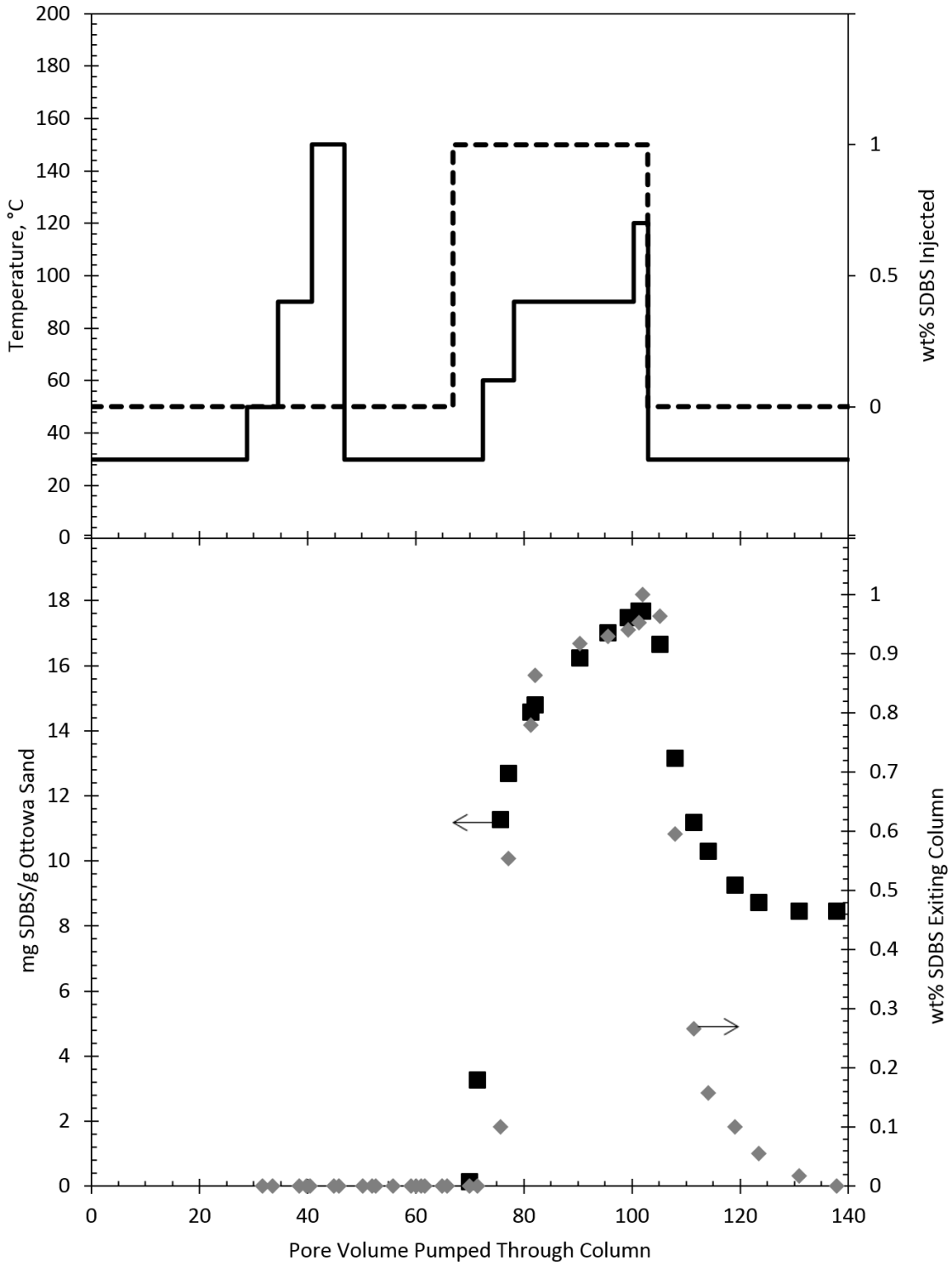

Figure 26: Experimental results from column filled with Ottawa sand and fracturing fluid of deionized water with 1 wt% SDBS. The top graph is the temperature of column (—) and wt% SDBS injected (---) versus pore volume pumped through column. The bottom graph is wt% SDBS exiting column (♦) and mg SDBS adsorbed/g Ottawa sand (■) versus pore volume injected. Arrows indicate which axis to read.

Experiments with DPDS are shown in Figure 27 through Figure 30. DPDS is a disulfonate surfactant and therefore the negative electrostatic charge is twice that of SDBS. The larger electrostatic repulsion is obvious when observing that there is almost a 50% decrease in apparent surfactant adsorption on Ottawa sand when comparing to SDBS. While the larger negative charge decreased adsorption for the negatively charged silica surface, it is clear the opposite would be true to a positive surface such as alumina.[65]

In Figure 27 through Figure 30, the concentration of NaCl increases from 0 to 20 wt% which appears to have no effect on the maximum adsorption density. This demonstrates the high salt tolerance of the DPDS surfactant. The large electrostatic repulsion between the two sulfonate groups and the negative aluminum surface appears to be unaffected by the increasing presence of counter ions.

An increase in temperature did not have an effect on the DPDS adsorption just as was observed in the ionic SDBS.

Because adsorption density is low for DPDS on Ottawa sand, it is hard to distinguish whether or not the apparent adsorption is an artifact of mixing effects within the column. However, the adsorption density being proportionally half with the presence of two sulfonate groups when compared to SDBS is encouraging and supportive of the data.

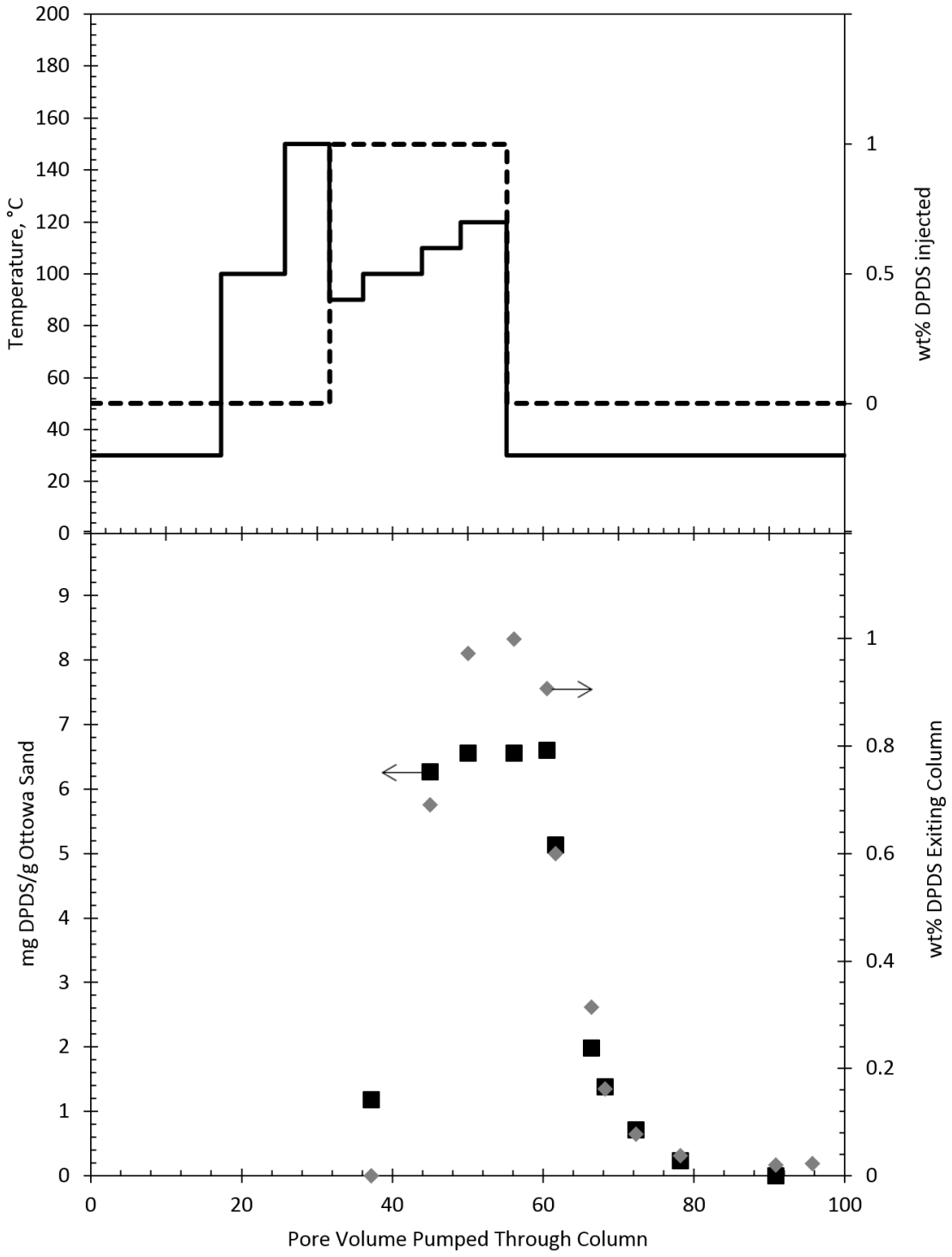

Figure 27: Experimental results from column filled with Ottawa sand and fracturing fluid of deionized water with 1 wt% DPDS. The top graph is the temperature of column (—) and wt% DPDS injected (---) versus pore volume pumped through column. The bottom graph is wt% DPDS exiting column (♦) and mg DPDS adsorbed/g Ottawa sand (■) versus pore volume injected. Arrows indicate which axis to read.

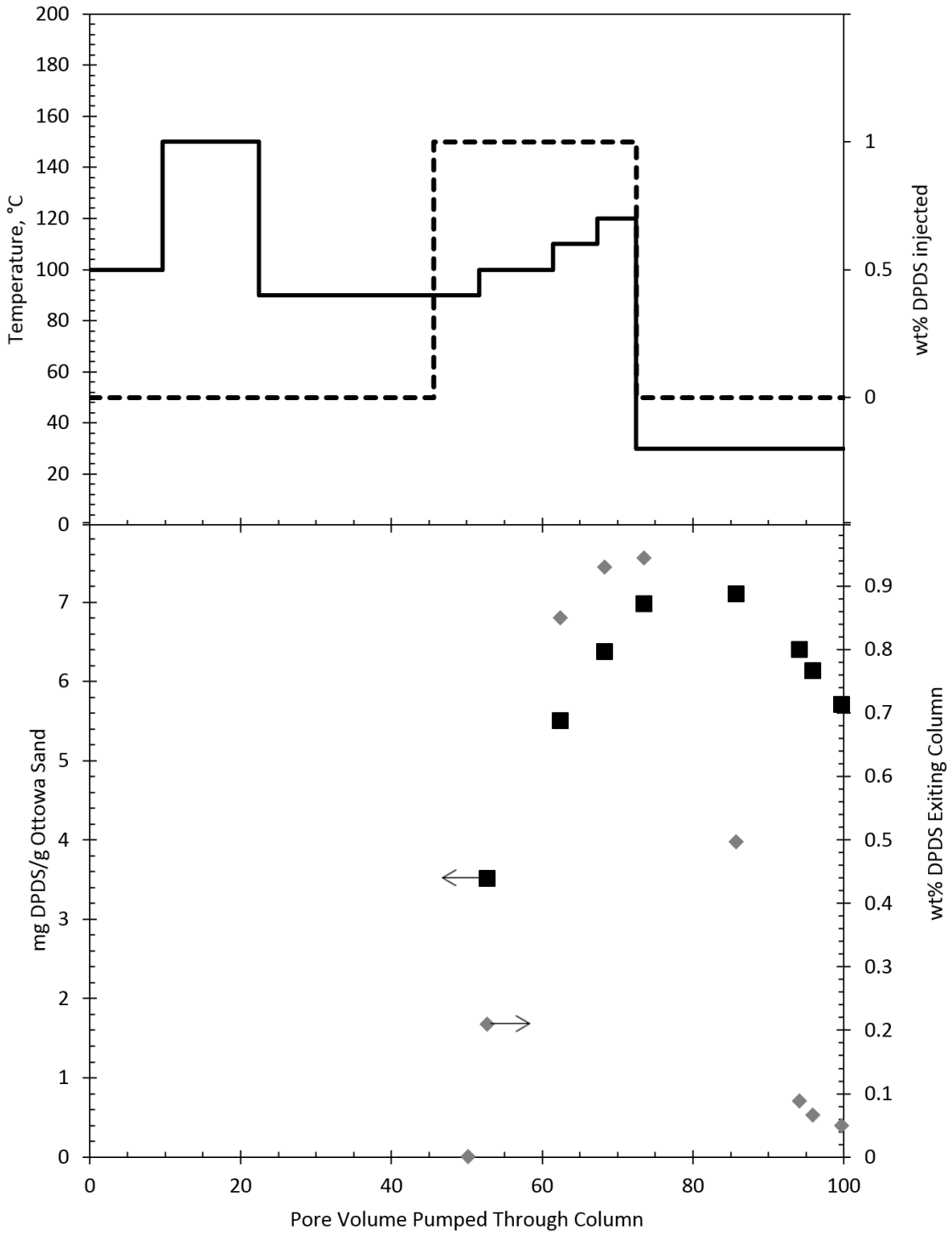

Figure 28: Experimental results from column filled with Ottawa sand and fracturing fluid with 1 wt% DPDS and 10 wt% NaCl. The top graph is the temperature of column (—) and wt% DPDS injected (---) versus pore volume pumped through column. The bottom graph is wt% DPDS exiting column (♦) and mg DPDS adsorbed/g Ottawa sand (■) versus pore volume injected. Arrows indicate which axis to read.

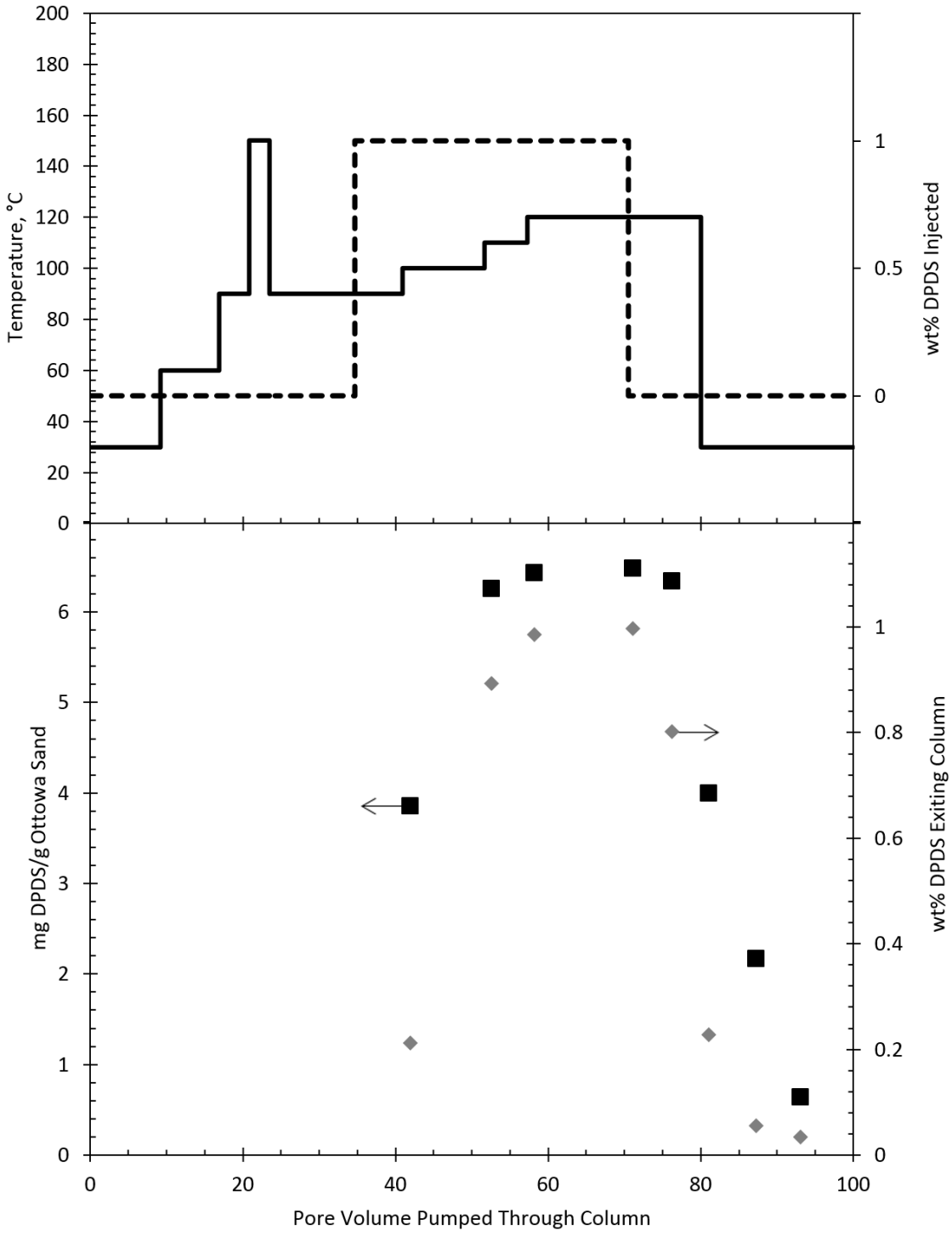

Figure 29: Experimental results from column filled with Ottawa sand and fracturing fluid with 1 wt% DPDS and 15 wt% NaCl. The top graph is the temperature of column (—) and wt% DPDS injected (---) versus pore volume pumped through column. The bottom graph is wt% DPDS exiting column (♦) and mg DPDS adsorbed/g Ottawa sand (■) versus pore volume injected. Arrows indicate which axis to read.

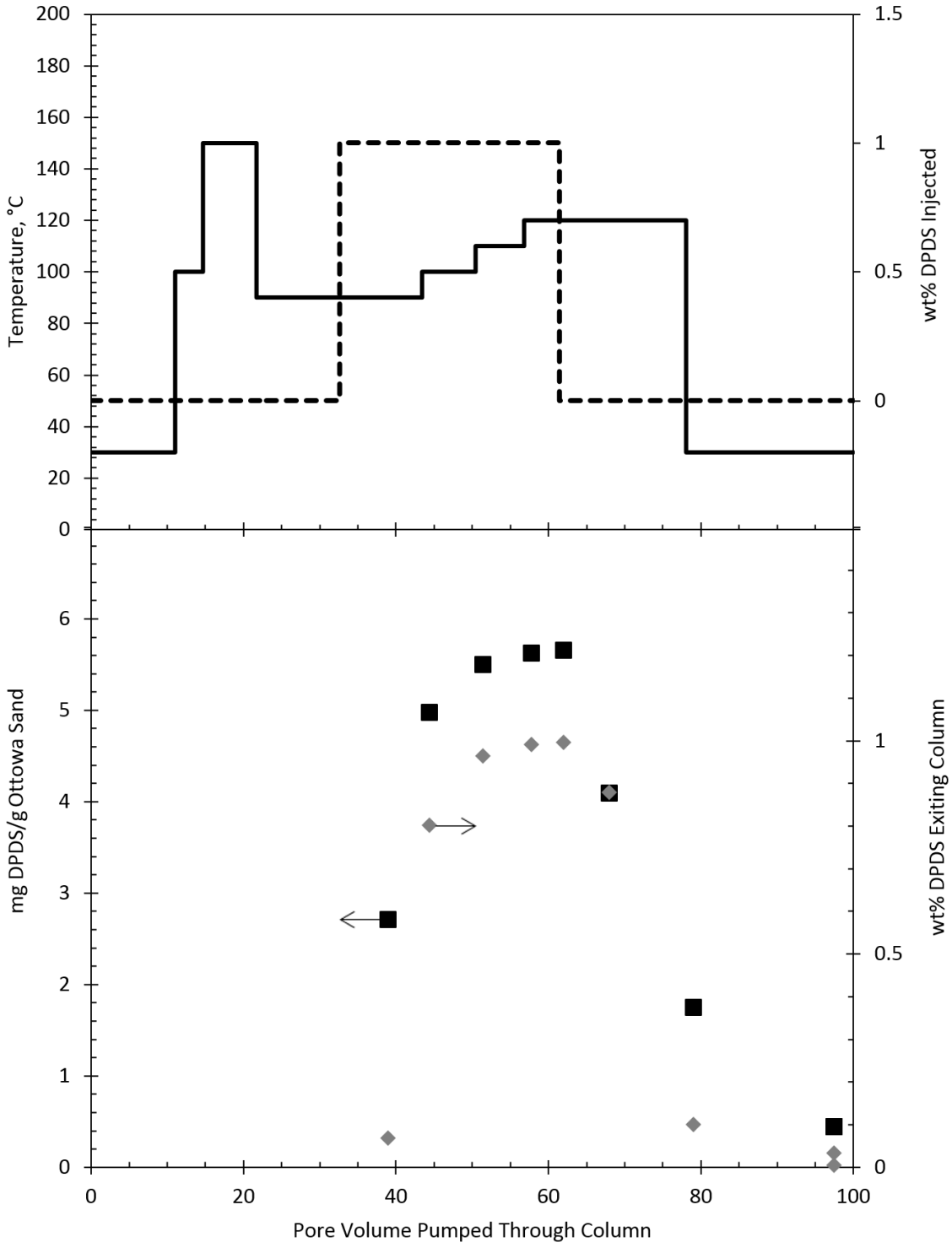

Figure 30: Experimental results from column filled with Ottawa sand and fracturing fluid with 1 wt% DPDS and 20 wt% NaCl. The top graph is the temperature of column (—) and wt% DPDS injected (---) versus pore volume pumped through column. The bottom graph is wt% DPDS exiting column (♦) and mg DPDS adsorbed/g Ottawa sand (■) versus pore volume injected. Arrows indicate which axis to read.

Conclusions

The high salinity and temperatures common in fracturing work cannot be neglected during fracturing formulation work. When the cloud point temperature of a nonionic surfactant is reached, the surfactant's migration through the rock matrix is severely limited due to coacervate formation. The high salinity increases adsorption for both ionic and nonionic surfactants, once again resulting in reduced chemical movement through the rock matrix. If these fracturing conditions are not taken into consideration for the fracturing fluid formulation, the resulting fluid will be unsuccessful in the field, and the potential of the compounds for migration in the subsurface will be greatly overestimated.

Chapter 4: Evidence for a Different Mechanism of Adsorption for Nonionic Surfactants with a High Degree of Ethoxylation

Introduction

Ethoxylated nonionic surfactants are a popular, widely used class of surfactants from enhanced oil recovery to household cleaning products to personal care items. In all of these scenarios, adsorption of the surfactant plays a key role in the product performance. Despite the popularity of these surfactants, a brief literature search will quickly reveal that a significant segment of these surfactants have received much less attention, as a large emphasis is placed on nonionic surfactants with a low degree of ethoxylation, less than 25 ethylene oxide units. Multiple papers[8-24] cover a wide range of topics regarding the adsorption of lower ethoxylated nonionic surfactants at the silica-water interface. Conversely, limited information is given about the adsorption behavior of highly ethoxylated surfactants, surfactants with more than 25 ethylene oxide units. A few papers discuss their adsorption isotherms[8,9,12,16] and adsorbed layer thickness using dynamic light scattering[18] at the silica-water interface, but overall, the literature is still lacking when compared to surfactants with a lower degree of ethoxylation.

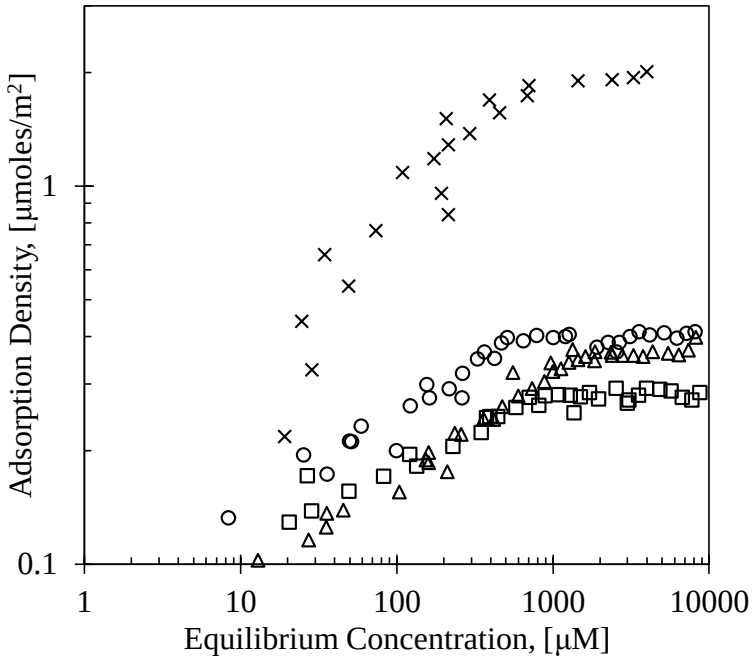

Figure 31: Adsorption isotherms for OP-40 (△), NP-40 (○), NP-55 (□), NP-10 (x) developed at 30°C in deionized water with fumed silica.[66]

When comparing adsorption isotherms for highly ethoxylated versus less ethoxylated nonionic surfactants, it is clear that a different mechanism of adsorption is occurring. Figure 31 shows adsorption isotherms for polyethoxylated octyl phenols, OP-X, and polyethoxylated nonyl phenols, NP-X, where X represents the degree of ethoxylation. A few papers suggest the difference in adsorption isotherm slopes is due to the presence or absence of hydrophobic association among alkyl tails.[8,41] The steep slope observed for NP-10 at low concentrations is due to the hydrophobic association among the alkyl tails of the surfactants adsorbing at the surface. The hydrophobic interaction allows for the formation of surface aggregates or a patchwise, bilayer-like coverage. The adsorption isotherms for OP-40, NP-40, and NP-55 do not have this low concentration steep slope because the long ethylene oxide groups create a steric hindrance to alkyl-alkyl association resulting in what is assumed to be monolayer

formation. Multiple studies have investigate less ethoxylated nonionic surfactants on a hydrophilic surface through ellipsometry[18,21-24,67] as well as at the air-water interface[68,69], the water-oil interface[70], and the water-hydrophobic surface interface[40], but no ellipsometry studies have been performed for highly ethoxylated nonionic surfactants whose adsorption densities are limited to monolayer formation.

Based on the idea of monolayer formation for highly ethoxylated nonionic surfactants, a mass action model was proposed for surfactants with a high degree of ethoxylation where one surfactant interacts with multiple surface sites on a hydrophilic surface.[41] At equilibrium,

$$\boldsymbol{p}\,\mathrm{S} + \mathrm{monomer} \rightleftarrows p\,\mathrm{S}^* \qquad \textbf{(14)}$$

and

$$K = \frac{a_{S^*}}{a_S a^{\frac{1}{p}}} \qquad \textbf{(15)}$$

where K is the equilibrium constant, p is the average number of surface sites, S, available to interact with a monomer, and S* is the occupied surface sites. This equilibrium assumption results in the adsorption isotherm equation,

$$\Gamma = \frac{\Gamma_\infty K c^{\frac{1}{p}}}{1 + K c^{\frac{1}{p}}} \qquad (16)$$

where Γ is the surfactant adsorption density at concentration, c, and Γ_∞ is the maximum surface excess concentration achievable only at infinite surfactant concentration.

This model for a high degree of ethoxylation is based on a low degree of ethoxylation model which works from the assumption that multiple surfactant monomers, n, are able to interact with a single surface site resulting in surface aggregates.[13]

$$\mathrm{S} + n\,\mathrm{monomer} \rightleftarrows \mathrm{surface\ aggregate} \qquad (17)$$

This present study aims to investigate the need for a unique mass action model for highly ethoxylated nonionic surfactants by confirming monolayer formation at the liquid-hydrophilic surface interface by means of ellipsometry and quartz crystal microbalance (QCM).

Materials

Polyethoyxlated (55) nonyl phenol, Surfonic NB-557, was supplied but Huntsman Corporation and polyethoxylated (10) nonyl phenol, Makon 10, was supplied by Stepan Company. All surfactants were used as received. These nonionic surfactants are polydisperse surfactants, with the distribution of ethylene oxides in the polymer chain described by a Poisson distribution. This paper refers to polyethoxylated nonyl phenols as NP-X where X represents the moles of ethylene oxide present in the surfactant.

Silicon with a thermally grown oxide layer, nominally 60 nm, was purchased from J.A. Woollam Co.

Q-Sense sensors, QSX 303 SiO_2, for the QCM were purchased from Biolin Scientific. The silicon dioxide layer was applied by physical vapor deposition and is 50 nm thick.

Methods

The ellipsometry instrument used in this study was a Gaertner Scientific Corporation, LSE Stokes Ellipsometer controlled by a computer using the Gaertner Ellipsometer Measurement Program (GEMP). All measurements were taken at a wavelength of $\lambda = 6382$ Å and an angle of incidence $\phi = 70°$.

For each experiment, a 1cm x 1 cm silicon dioxide wafer was cleaned with a 5 minute acetone sonication bath and blown dry with nitrogen, followed by a 5 minute methanol sonication bath and blown dry with nitrogen. The integrity of the surface was visual confirmed using a Nikon differential interface contrast (DIC) microscope. The oxide layer thickness was then confirmed with an ellipsometry measurement in air at room temperature, 22°C. Each ellipsometry measurement recorded the angles ψ and Δ. The GEMP software also used a two layer model to report the mean optical thickness and the refractive index for the surfactant layer. For cleaned oxidized silicon pieces and *ex situ* ellipsometry measurements, data was recorded in five different locations on the wafer. A schematic of the five approximate locations marked A through E, performed in that order, is shown in Figure 32. For *in situ* measurements, all ellipsometry measurements were focused only in the center of the oxidized silicon wafer because the set up did not allow for easy manipulation of the wafer.

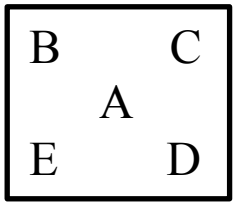

Figure 32: Schematic of where *ex situ* ellipsometry measurements were performed. Location are marked alphabetically and were performed in that order.

Ex situ ellipsometry measurements were performed after allowing surfactant from an aqueous solution, at 2 x CMC, to adsorb on the cleaned oxidized silicon wafer for one hour. While keeping the surface wet, the wafer with adsorbed surfactant was transferred to a beaker with deionized water and the wafer was gently rinsed for 5 minutes with deionized water. While still keeping the surface wet, the wafer was transferred to a Laurell WS-200 spin coater to be spun for 1 minute at 3000 rpm until

dry. The surface was visually observed with the Nikon DIC microscope and ellipsometry measurements were performed in air at 22°C. The oxidized silicon wafer with adsorbed surfactant was then transferred to a deionized water sonication bath for 10 minutes, ozone cleaning for 5 minutes, and plasma cleaning for 5 minutes. After the deionized water sonication bath and in between each cleaning step, the same spin drying procedure, DIC microscope observations, and ellipsometry measurements were performed.

In situ measurements were performed by using a metal prism purchased from Gaertner Scientific which had an open top and interior dimensions of 2.3 x 2.3 x 1.7 cm. Two windows are located on opposite ends of the prism to allow for ellipsometry measurements. A schematic of the prism is shown in Figure 33.

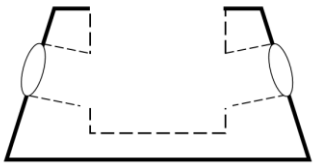

Figure 33: Schematic of Gaertner Scientific Prism for *in situ* measurements

For *in situ* measurements, the cleaned oxidized silicon wafer was placed in the prism and ellipsometry measurements were taken in air at room temperature. The prism was then filled with a known amount of deionized water and ellipsometry measurements were repeated. A known amount of 10^{-2} M surfactant was injected in the top of the prism to result in a surfactant concentration 2 x CMC and ellipsometry measurements were taken once every ten seconds for two hours. The injected surfactant was allowed to disperse naturally, as any stirring would shift the oxidized silicon wafer and misalign the lasers of the ellipsometer.

All collected data was analyzed using the GEMP software.

The Q-Sense sensors were cleaned according to Biolin Scientific's recommended cleaning method.[71] The sensors were treated with UV/ozone for 10 minutes then immersed in a 2 wt% sodium dodecyl sulfate solution at room temperature for 30 minutes. The sensors were then rinsed with milliQ water and then blown dry with nitrogen. Lastly, the sensors were UV/ozone treated for another 10 minutes.

The Q-Sense sensors were placed in a Q-Sense Model E 4 QCM. The system temperature was set to 30°C and liquid flow set to 0.1 mL/min. Initially, milliQ water was pumped through the QCM, followed by NP-55 at concentrations 0.3, 0.5, 0.7, 1, 1.5, and 2 x CMC. The CMC of NP-55 is 465 μM.[42] Each liquid was pumped through the system until the sensor frequency change was less than ± 0.3 Hz.

All QCM data was analyzed using the Voigt model and Biolin Scientific's QTools. To account for error due to the presence of water in the adsorbed layer, a correction factor was added to the QTools's model fitted mass output. This correction factor was determined by matching the adsorption densities at 2 x CMC.

Results and Discussion

Figure 34 and Figure 35 show the ellipsometry results of the measurements for NP-10 and NP-55, respectively, performed *ex situ*. Across the stages of the adsorption-desorption process, the adsorbed layer thickness of NP-10 is always larger than the thickness of NP-55. The difference in thickness suggests a difference in surfactant arrangement at the surface.

Other studies have suggested that surfactants with short ethylene oxide chains, less than 25 ethoxylate units, have an adsorbed layer thickness of approximately twice the alkyl chain length, which corresponds to bilayer formation. This would indicate the

adsorbed layer thickness of NP-10 would be approximately 30 Å which is the case for spots A and B in Figure 34 after surfactant adsorption. Spots C through E did not have as high of a surfactant layer thickness. This is most likely due to the deionized water rinse desorbing some of the surfactant, resulting in an incomplete bilayer. The incomplete bilayer is further destructed with the deionized water sonication bath; afterwards the average adsorbed layer thickness is approximately 15 Å which indicates that the bilayer has almost completely been removed and only a monolayer remains.

At this point, the sample was allowed to rest in air at 22°C for 12 hours. After the 12 hour period, the NP-10 adsorbed layer still has an adsorbed thickness of approximately 15 Å. The slight shift between data points can be attributed to the manual positioning of the wafer when taking ellipsometry measurements. Finally, the UV cleaning and the O_2 plasma cleaning appear to remove almost all of the surfactant from the surface.

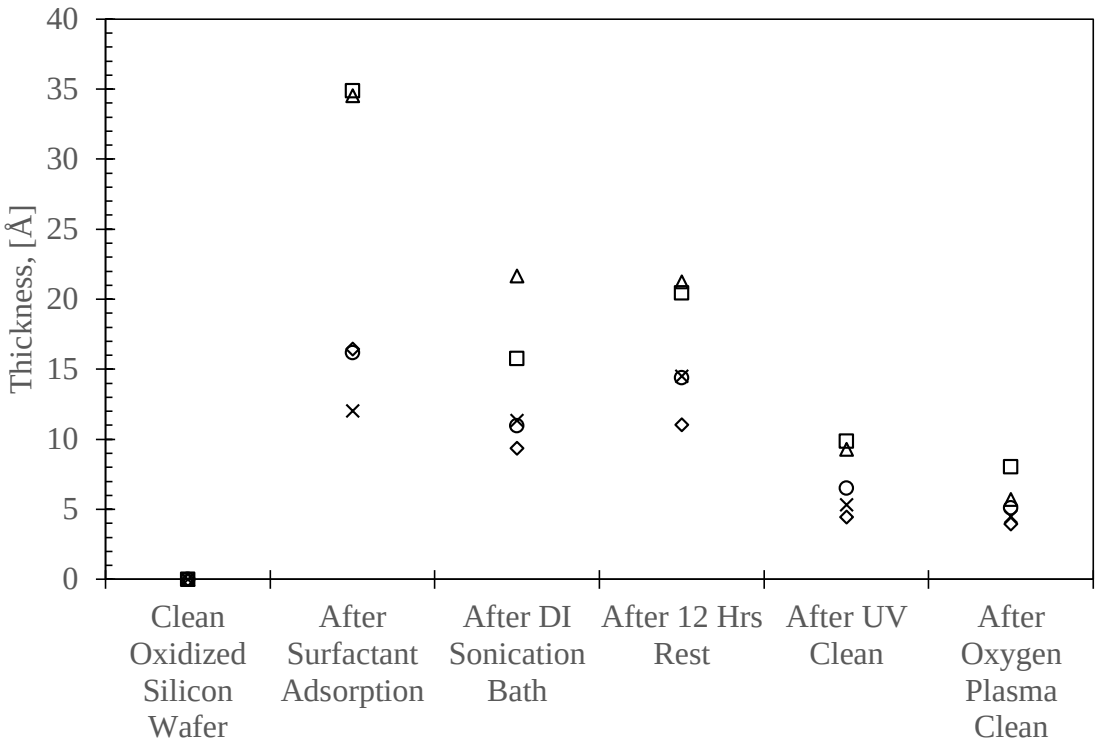

Figure 34: *Ex situ* ellipsometry results for NP-10 on oxidized silicon in air at 22°C versus the timeline of the adsorption-desorption process. Five measurements were taken on the same wafer in locations A (□), B (△), C (x), D (◇), and E (○), see Figure 32.

The adsorbed surfactant layer for NP-55 in Figure 35 is less than the proposed monolayer thickness, 15 Å, at every stage of the adsorption/desorption process. Note the different scale of the vertical axis between Figure 34 and Figure 35. After surfactant adsorption, the adsorbed layer for the NP-55 surfactant in Figure 35 is less than 5 Å which suggests that the surfactant molecules are lying flat on the surface, as reported ethylene oxide polymers have a similar reported layer thickness.[18] The effect from the deionized water sonication bath is not as dramatic as compared to NP-10 since the adsorbed layer is already less than 5 Å and the variation in height difference between spots may be attributed to the manual set up of the ellipsometer. This may also reflect the greater difficulty in desorbing the long PEG chain by rinsing with water because the

PEG chain is attached to multiple adsorption sites on the surface. The increased thickness variation after the 12 hour rest period may be due to impurities on the surface or, once again, human error due to the manual set up of the ellipsometer; alternatively, there may be some unknown mechanism that leads to an adsorbed layer thickness increase with the sonication and aging of the surface. Finally, the UV cleaning and O_2 plasma cleaning removed the surfactant from the surface.

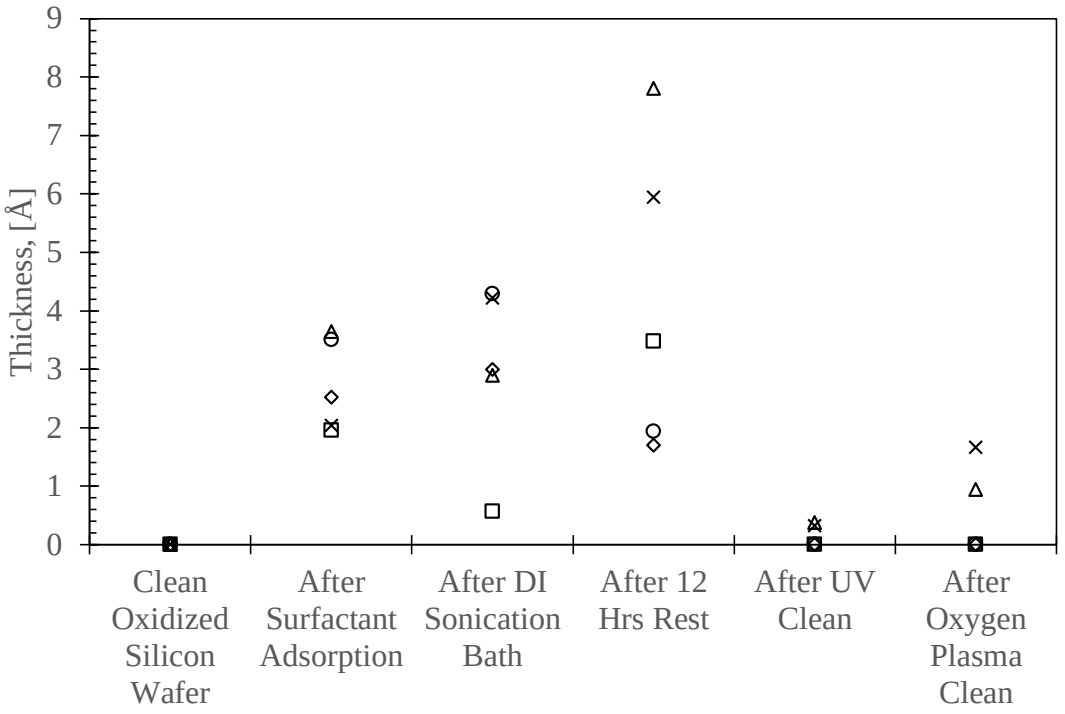

Figure 35: *Ex situ* ellipsometry results for NP-55 on oxidized silicon in air at 22°C versus the timeline of the adsorption-desorption process. Five measurements were taken on the same wafer in locations A (□), B (△), C (x), D (◇), and E (○), see Figure 32.

In situ ellipsometry results are shown in Figure 36 and Figure 37. The recorded ψ and Δ values from the GEMP software had to be manual adjusted to account for the error resulting from the reflectance/transmittance of the ellipsometer light source from the glass windows of the prism and the water. The shift in ψ and Δ values was found to be quantifiable. The combined effect from the glass windows and the water was found

to shift the ψ values 15° lower and the Δ values 12° higher. Without this corrective factor, the film thickness was consistently overestimated. This corrective factor was tested with two different oxidized silicon samples. *Ex* situ ellipsometry compared with *in* situ ellipsometry resulted in a less than 4% error when this corrective factor for ψ and Δ was applied. The results reported in Figure 36 and Figure 37 are based on the GEMP software calculations using the corrected ψ and Δ values.

Similar to the *ex situ* ellipsometry results, the *in situ* results also show a distinct difference between layer thicknesses of NP-10 and NP-55, with the NP-10 adsorbed layer being larger than the NP-55 adsorbed layer. Both *in situ* results are also higher than their *ex situ* results, suggesting that hydration of the surfactant layer contributes to its layer thickness.

The final adsorbed layer thickness of NP-10 shown in Figure 36 is approximately 38 Å which is larger than the predicted thickness of 30 Å based on a series of hexa(ethylene glycol) monoalkyl ethers with varying hydrocarbon tail lengths. The increased thickness may suggests the slightly larger hydrated ethylene oxide groups, ten versus six, contributes more to the adsorbed layer thickness. The step-like change in adsorbed layer thickness after 15 minutes, from slightly less than 20 Å to nearly 40 Å is interesting, since this step is approximately half the final adsorbed layer thickness, suggesting a transition from a monolayer to a bilayer as adsorption proceeds. However, this step could also be an artifact of the GEMP software modeling since the surfactant was injected at the top of the prism and allowed to diffuse to the oxidized silica surface.

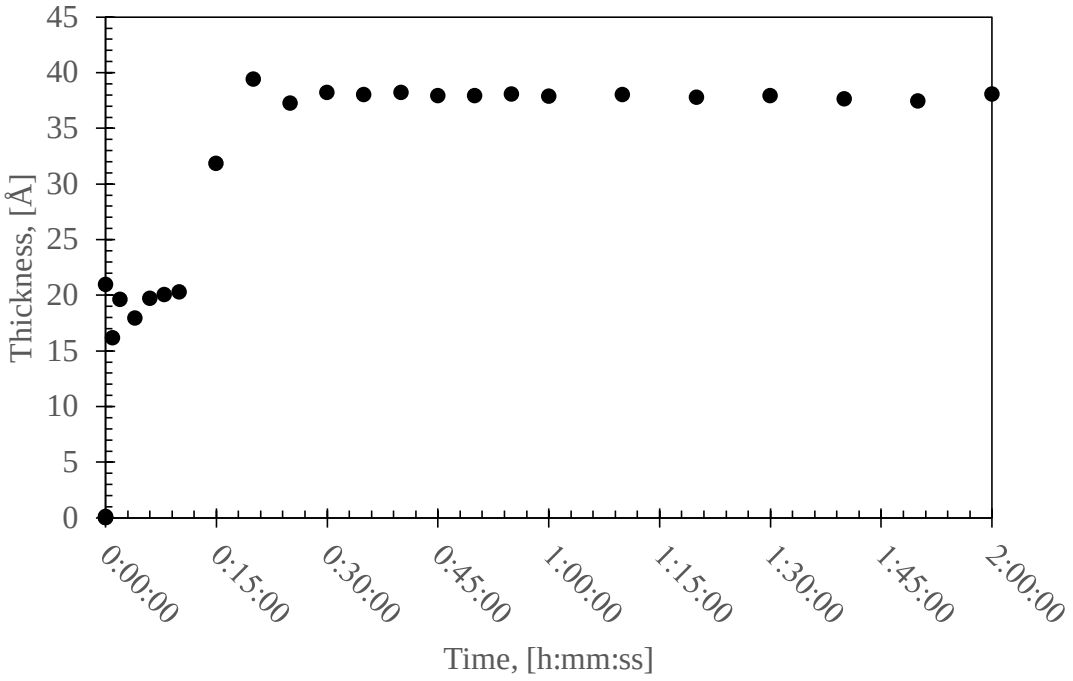

Figure 36: *In situ* ellipsometry results for NP-10 on oxidized silicon at 22°C versus time.

The adsorption of NP-55 surfactant occurred quickly, in less than 6 minutes, and did not change much over the next two hours. The final adsorbed layer thickness was approximately 23 Å which is significantly larger than the *ex situ* results. This further emphasizes that the hydration of the ethylene oxide groups of the surfactants plays a significant role in the adsorbed layer thickness. Additionally, the height of this layer suggest that the entire head group of this ethoxylated surfactant may not be laying complete flat on the surface, since the tail length is estimated to be only 15 Å.

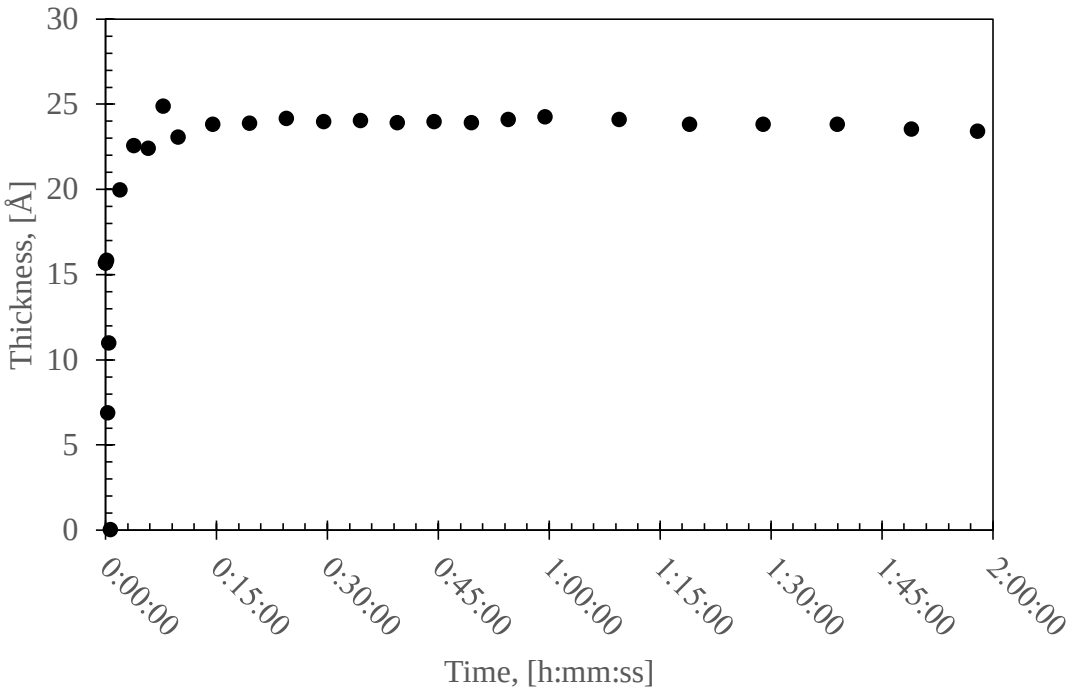

Figure 37: *In situ* ellipsometry results for NP-55 on oxidized silicon at 22°C versus time.

QCM data, Figure 38, was able to confirm the adsorption density of NP-55 on silica at 30°C in deionized water. Both QCM analysis and UV analysis confirm a lower adsorption density on silica for NP-55 compared to NP-10 adding further evidence that a different mechanism of adsorption is occurring with the more highly ethoxylated nonionic surfactants. The QCM data shows a large change in dissipation once NP-55 was introduced to the system which indicates a soft film has been adsorbed to the sensor's surface. This soft film can be interpreted as the ethoxylated chain of the NP-55 surfactant not fully or rigidly binding to the surface, but instead binding in a polymer-like fashion as loops, trains, and tails.[72,73] The hydrophobic carbon tails not bonding with the hydrophilic silica surface or being able to participate in bilayer formation may also be contributing to the large dissipation.

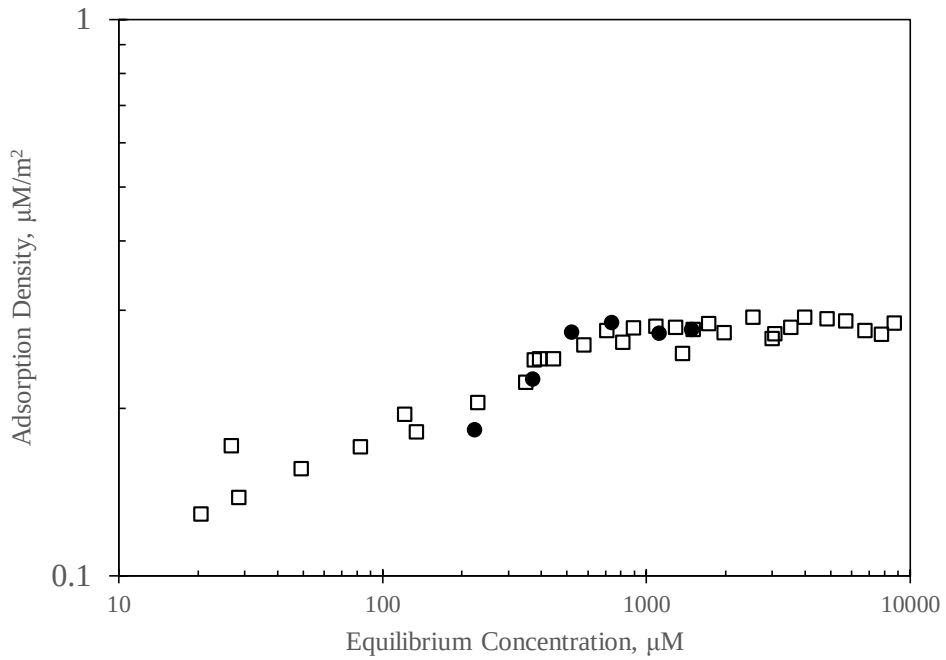

Figure 38: Adsorption isotherms for NP-55 in deionized water at 30°C developed on fumed silica and analyzed with UV analysis at 224 nm (□)[66] and developed on a plated silica sensor and analyzed with a QCM (●).

Based on the UV analysis, ellipsometry, and QCM results, the need for a unique mass action model for highly ethoxylated nonionic surfactants appears to be validated. Figure 39 shows the data in Figure 31 with the mass action model overlaid. The model appears to accurately reflect the maximum adsorption density as both NP-40 and OP-40 are approaching 0.43 µmoles/m^2 and the adsorption density for NP-55 is approaching 0.28 µmoles/m^2. These adsorption densities are dramatically different from NP-10 which appeared to be approaching 2.00 µmoles/m^2 in Figure 31. This is in agreement with literature that the adsorption density for ethoxylated nonionic surfactants on a hydrophilic surface is inversely proportional to the number of ethylene oxide units.[8-11]

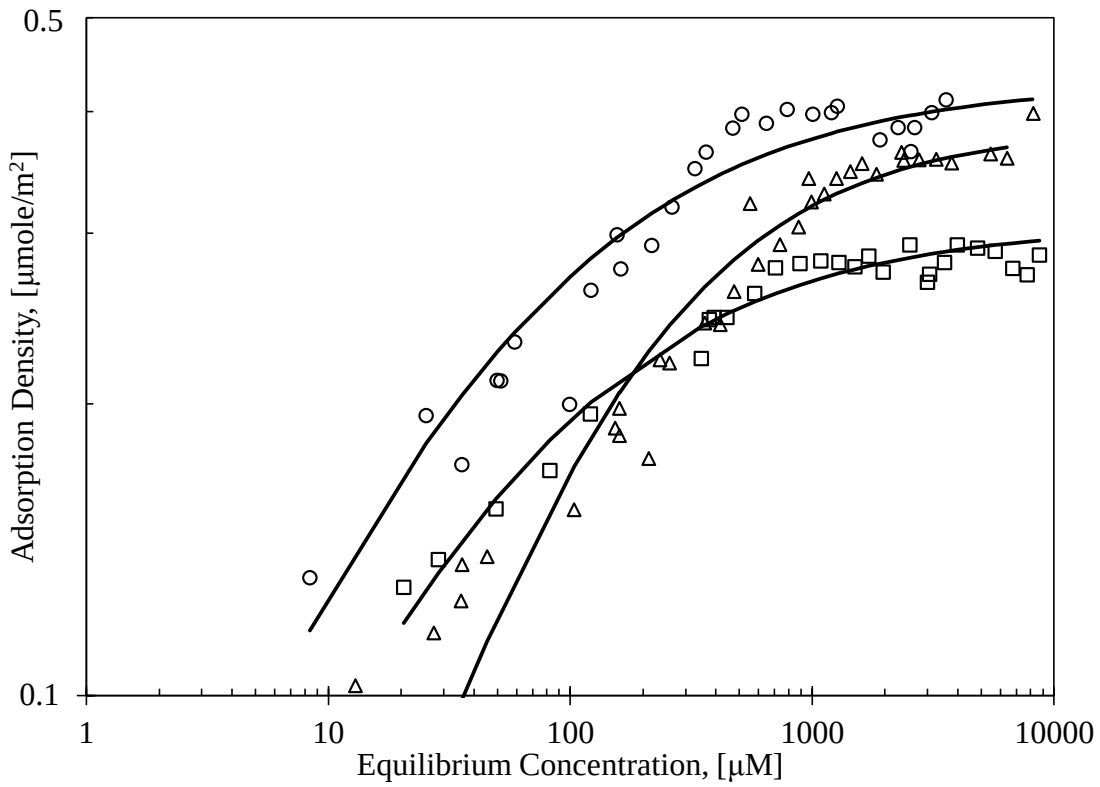

Figure 39: Adsorption isotherms for OP-40 (△), NP-40 (○), and NP-55 (□) developed at 30°C in deionized water with fumed silica with mass action model overlay.

Conclusions

Ellipsometry and QCM results both support the idea of a difference in adsorption mechanism between low and high ethoxylated nonionic surfactants. Low ethoxylated nonionic surfactants adsorb on a hydrophilic surface as aggregates because their small ethoxylated head group allows for hydrophobic association among their tails. Highly ethoxylated nonionic surfactants adsorb as monolayers because their large ethoxylated head group does not allow for surface aggregate formation and instead monolayer formation occurs with the large ethoxylated chains in contact with the oxidized silicon surface. Overall, this results in nonionic surfactants with a low degree of ethoxylation having a higher adsorption density than nonionic surfactants with a high degree of ethoxylation. This idea should not be neglected when working with

ethoxylated surfactants since drastically different results can occur based on the ethoxylated chain length. The *in situ* ellipsometry results indicate the adsorbed layer thickness is also affected by hydration and this is especially apparent in the highly ethoxylated surfactant. The *ex situ* results for the less ethoxylated surfactant suggest that the adsorbed layer may have been affected by the deionized water rinsing, resulting in a dewetting phenomenon on the surface. The QCM results suggest a soft, non-rigid surfactant adsorbed layer and confirm the adsorption density previously obtained through UV analysis. With the ellipsometry results showing an adsorbed layer thickness of slightly longer than the alkyl tail for NP-55, as well as the QCM results showing a soft adsorbed layer, the adsorption of high ethoxylated nonionic surfactants may be more similar to polymer adsorption than low ethoxylated surfactant adsorption.

Chapter 5: Closing Remarks

Nonionic surfactants with a high degree of ethoxylation are affected by the presence of salts and this effect depends on the ions present and the concentration of these ions. In Chapter 2, adsorption densities were shown to be low, which hints at monolayer formation, and independent of the alkyl chain length. The presence of a salt either increased or decreased the maximum adsorption density and this effect was proportional to the concentration of the salt. Classification of ion effects matched well with the Hofmeister series. The ability to manipulate the adsorption density based on the ion present in solution is very useful in applications where project success or failure is based on chemical interaction at the solid-liquid interface, such as enhanced oil recovery or household cleaning products. Such an application was shown in Chapter 3 where the presence of sodium chloride increased adsorption loss for NP-55 from a fracture fluid when flowing through shale or sand packed column. Furthermore, the presence of sodium chloride decreased the cloud point of NP-55 causing coacervate formation which resulted in almost none of the surfactant traveling through to the end of the packed column. By comparison with ionic surfactants, high salt and temperature tolerance was the clear factor in determining successful migration through the packed column, as seen with DPDS.

Finally, the difference in maximum adsorption densities depending on the nonionic surfactant's degree of ethoxylation seen in Chapter 2 was revised in Chapter 4. In building the case for a different mechanism of adsorption for high versus low ethoxylated nonionic surfactants, ellipsometry was performed which confirmed adsorbed layer height differences between two surfactants with the same alkyl length

but different degrees of ethoxylation. NP-55 showed a lower adsorbed layer height compared to NP-10 which suggested that NP-10 was able to adsorb in bilayer-like fashion. The adsorbed layer thickness for NP-55 was at first suspected to monolayer formation with a height dependent on the length of the alky tail, but ellipsometry results showed a height greater than the length of the alkyl tail. QCM results confirmed the maximum adsorption density for NP-55 on a hydrophilic silica surface as well as showing a soft, non-rigid adsorbed layer. The knowledge of a soft non-rigid adsorbed layer coupled with the ellipsometry results for an adsorbed height greater than the length of the alky tail suggest the high ethoxylated nonionic surfactant is adsorbing in a polymer like fashion. This confirms the need for a different mechanism of adsorption based on the long ethoxylate chain interacting with more of the surface compared to a short EO chain and resulting in a stearic hindrance preventing hydrophilic association.

References

[1] Miller, L. S. *Science* **1953**, *117*, 528-529.

[2] Miller, L. S.; Harold, U. C. *Science* **1959**, *130*, 245-251

[3] Chemical Use in Hydraulic Fracturing. https://fracfocus.org/water-protection/drilling-usage (accessed August 22, 2014).

[4] *Evaluation of Impacts to Underground Sources of Drinking Water by Hydraulic Fracturing of Coalbed Methane Reservoirs*, "Hydraulic Fracturing Fluids", US EPA 816-R-04-003, June 2004

[5] *Proceedings of the Technical Workshops for the Hydraulic Fracturing Study: Fate and Transport*, US EPA 600/R-11/047, May 2011.

[6] Beunen, J. A.; Ruckenstein, E. *Adv. Colloid Interface Sci.* **1982**, *16*, 201-231.

[7] Bourrel, M.; Koukounis, Ch. Schecter, R.; Wade, W. *J. Disp. Sci. Tech.* **1980**, *1*, 13-35.

[8] Somasundaran, P.; Snell, E. D.; Xu, Q. *J. Colloid Interface Sci.* **1991**, *144*, 165-173.

[9] Partyka, S.; Zaini, S.; Lindheimer, M.; Brun, B. *Colloids Surf.* **1984**, *12*, 255-270.

[10] Lindheimer, M.; Keh, E.; Zaini, S.; Partyka, S. *J. Colloid Interface Sci.* **1990**, *138*, 83-91.

[11] Levitz, P.; van Damme, H.; Keravis, D. *J. Phys. Chem.* **1984**, *88*, 2228-2235.

[12] Denoyel, R.; Rouquerol, J. *J. Colloid Interface Sci.* **1991**, *143*, 555-572.

[13] Gu, T.; Zhu, B. *Colloids Surf.* **1990**, *44*, 81-87.

[14] Somasundaran, P.; Middleton, R.; Viswanathan, K. V. *Relationship Between Surfactant Structure and Adsorptionin Structure/ Performance Relationships in*

Surfactants; Rosen, M. J., Ed.; American Chemical Society: Washington, D.C., **1984**; *253*, 269-290.

[15] Singh, S. K.; Notley, S. M. *J. Phys. Chem. B*. **2010**, *114*, 14977-14982.

[16] Misra, P. K.; Mishra, B. K.; Somasundaran, P. *J. Colloid Interface Sci.* **2003**, *265*, 1-8.

[17] Rutland, M. W.; Senden, T. J. *Langmuir* **1993**, *9*, 412-418.

[18] Bohmer, M. R.; Koopal, L. K.; Janssen, R. *Langmuir* **1992**, *8*, 2228-2239.

[19] Thritle, P. N.; Li, Z. X.; Thomas, R. K. *Langmuir* **1997**, *13*, 5451-5458.

[20] Grant, L. M.; Tiberg, F.; Ducker, W. A. *J. Phys Chem. B.* **1998**, *10*, 4288-4294.

[21] Tiberg, F.; Jönsson, B.; Lindman, B. *Langmuir* **1994**, *10*, 3714-3722.

[22] Brinck, J.; Jönsson, B.; Tiberg, F. *Langmuir* **1998**, *14*, 1058-1071.

[23] Tiberg, F.; Landgren, M. *Langmuir* **1993**, *9*, 927-932.

[24] Tiberg, F.; Jönsson, B; Tang, J.; Lindman B. *Langmuir* **1994**, *10*, 2294-2300.

[25] Fineman, M. N.; Brown, G. L.; Myers, R. J. *J. Phys Sci.* **1952**, *56*, 963-966.

[26] Hsiao, L.; Dunning H. N.; Lorenz, P. B. *J. Phys. Chem.* **1956**, *60*, 657-660.

[27] Becher, P. *J. Colloid Interface* **1962**, *17*, 325-333.

[28] Santos, F. K.; Neto, E. L.; Moura, M. C.; Dantas, T. N.; Neto, A. A. *Colloids Surf. A: Physicochem. Eng. Aspects* **2009**, *333*, 156-162.

[29] Schott, H. *J. Colloid Interface* **1995**, *173*, 265-277.

[30] Schott, H.; Han, S. K. *J. Pharm. Sci.* **1976**, *65*, 975-978.

[31] Kalra, A.; Tugeu, N.; Cramer, S. M.; Harde, S. *J. Phys. Chem. B.* ***2001***, *105, 6380-6386*.

[32] Rosen, M. J. *Surfactants and Interfacial Phenomena*, 3rd ed.; Wiley Interscience: Hoboken, 2004.

[33] Schott, H. Royce, A. E.; Han, S. K. *J. Colloid Interface* **1984**, *98*, 196-201.

[34] Li, J.; Bai, D.; Chen, B. *Colloid Suf. A* **2009**, *346*, 237-243.

[35] Mukherjee, P.; Padhan, S. K.; Dash, S.; Patel, S.; Mishra, B. K. *Adv. Colloid Interface Sci.* **2011**, *162*, 59-79.

[36] Schott, H. *Colloid Surf.* **2001**, *186*, 129-136.

[37] Vlanchy, N.; Drechsler, M.; Verbavatz, J.; Touraud, D.; Kunz, W. *J. Colloid Interface* **2008**, *319*, 542-548.

[38] Zhang, Y.; Cremer, P. *Curr. Opin. Chem. Bio.* **2006**, *10*, 658-663.

[39] Schott, H. J. *Colloid Interface* **1997**, *189*, 117-122.

[40] Kumar, N.; Garoff, S.; Tilton, R. D. *Langmuir* **2004**, *20*, 4446-4451.

[41] Goodwin, D. A. Jr. M.S. Thesis, The University of Oklahoma, OK, November 2012.

[42] Baker, D. K.; Goodwin, D. A. Jr.; Harwell, J. H., *upon submission*

[43] Shen, Y. *Chemosphere* **2000**, *41*, 711-716.

[44] Sanchez-Martin, M. J.; Dorado, M. C.; Del Hoyo, C.; Rodrigquez-Cruz, M. S. *J. Hazard Mater.* **2008**, *105*, 115-123.

[45] Blom, Annabelle; Warr, Gregory G.; Wanless, Erica J. *Langmuir*. **2005**, *21*, 11850-11855.

[46] McDermott, D.C.; Lu, J. R.; Lee, E. M.; Thomas, R.K. *Langmuir*. **1992**, *8*, 1204-1210

[47] Baker, D.K.; Rassel, S.M.S.S.; Johnson, M.B.; Harwell, J.H., *upon submission*

[48] *The Natural Energy Modeling System Oil and Gas Supply Module*. Technical Report of the U. S. Energy Information Administration: September 2015.

[49] Dresel, P. E.; Rose, A. W. *Chemistry and Origin of Oil and Gas Well Brines in Western Pennsylvania*; Open-File Oil and Gas Report for Pennsylvania's Department of Conservation and Natural Resources: Harrisburg, PN, 2010.

[50] Chaplin, M. Hofmeister Series. [Online] http://www1.lsbu.ac.uk/water/hofmeister_series.html (Accessed November 15, 2015).

[51] Koop, T.; Luo, B.; Tsias, A.; Peter, T. *Nature* **2000**, *406*, 611-614.

[52] Baker, D.K.; Goodwin, D.A. Jr; Harwell, J.H. *upon submission*

[53] Biosurfaces: Water Structure at Interfaces Part 1 (Nanotechnology). what-when-how, http://what-when-how.com/nanoscience-and-nanotechnology/biosurfaces-water-structure-at-interfaces-part-1-nanotechnology/ (accessed Mar 14, 2016).

[54] Dutzik, T.; Ridlington, E.; Rumpler, J. The Cost of Fracking: The Price of Dirty Drilling's Environmental Damage. [Online] **2012**. http://www.frontiergroup.org/sites/default/files/reports/The%20Costs%20of%20Fracking%20vUS.pdf (accessed December 12, 2015)

[55] Terracina, J. M.; Turner, J. M.; Collins, D. H.; Spillars, S. E. *SPE*, **2010**, *SPE 135502*, 1-17.

[56] Yoxtheimer, D. Water Treatment Solutions for Marcellus Natural Gas Development. In *Legislative Information Session*, Marcellus Center for Outreach and Research, Penn State, Aug 2010.

[57] Lv, W.; Bazin, B.; Ma, D.; Liu, Q.; Han, D.; Wu, K. *J. Petrol. Sci. Eng.* **2011**, *77*, 209-218

[58] Azam, M. R.; Tan, I. M.; Ismail, L.; Mushtaq, M.; Nadeem, M.; Sagir, M. *J. Petrol. Explor. Prod. Technol.* **2013**, *3*, 195-201

[59] Trogus, F. J.; Sophany, T.; Schechter, R. S.; Wade, W. H. *J. Soc. Petrol. Eng* **1977**, *17*, 337-344

[60] Grigg, R. B.; Bai, B. *SPE Int. Symp. Oilfield Chem.* **2005**, *SPE93100*, 1-12

[61] Misra, P. K.; Mishra, B. K.; Somasundaran, P. *J. Colloid Interface Sci.* **2003**, *265*, 1-8.

[62] Baker, D. K.; Goodwin, D. A. Jr.; Harwell, J, H. *upon submission*.

[63] Tadros, T. F. *J. Colloid and Interface Sci*. **1974**, *46*, 528-540.

[64] Bremmell, K. E.; Jameson, G. J.; Biggs, S. *Colloids and Surfaces A.* **1999**, *146*, 75-87.

[65] Neupane, D.; Park, J. W. *Chemosphere*. **1999**, *38*, 1-12.

[66] Baker, D.K; Goodwin, D.A. Jr; Harwell, J.H. *upon submission*

[67] Luciani, L.; Denoyel, R. *Langmuir*, **1997**, *13*, 7301-7303.

[68] Colin, A.; Giermanska-Kahn, J.; Langevin, D.; *Langmuir* **1997**, *13*, 2953-2959.

[69] Goates, S.R.; Schofield, D.A.; Bain, C.D. *Langmuir* **1999**, *15*, 1400-1409.

[70] Benhamins, J.W.; Thuresson, K.; Nylander, T. *Langmuir*, **2005**, *21*, 149-159.

[71] *Q-Sense Sensor QSX 303 SiO_2*, Biolin Scientific, Production Specifcations.

[72] Hoeve, C.A.J. *J. Polym Sci*, **1970**, *30*, 361-367.

[73] Trens, P.; Denoyel, R. *Langmuir*, **1993**, *9*, 519-522.